

U-Pb zircon ages of the Wildhorse gneiss, Pioneer Mountains, south-central Idaho, and tectonic implications

Paul K. Link¹, Kathleen M. Autenrieth-Durk¹, Angie Cameron¹, C. Mark Fanning², James J. Vogl³, and David A. Foster³

¹Department of Geosciences, Idaho State University, Pocatello, Idaho 83209, USA

²Research School of Earth Sciences, Australian National University, Canberra, ACT 0200, Australia

³Department of Geosciences, University of Florida, Gainesville, Florida 32611, USA

ABSTRACT

The gneiss complex of Wildhorse Creek (Wildhorse gneiss) forms the central component of the lowest structural plate in the Pioneer metamorphic core complex of south-central Idaho. The oldest rock in the complex is a felsic orthogneiss, with Neoproterozoic U-Pb magmatic zircon ages of 2.60–2.67 Ga. The orthogneiss overlaps in age and is interpreted to be part of the Grouse Creek block of the Albion Mountains to the south. This Archean metagranitoid is structurally interleaved with paragneiss containing quartzite and calc-silicate rock. Structurally below the orthogneiss, some quartzites have multiple concordant populations of detrital-zircon grains as young as ca. 1700 Ma, while others have no zircon grains younger than ca. 2500 Ma.

Structurally above the Archean gneiss is a heterogeneous paragneiss that contains calc-silicate and quartzitic rocks with detrital zircons as young as ca. 1460 Ma. Amphibolite in this unit contains zircons dated at ca. 1850 Ma, indicating that this rock can be no older than that and implying considerable structural complexity. The upper part of the Wildhorse gneiss contains metaquartzites bearing zircons as young as ca. 1400 Ma. The protolith of this paragneiss is interpreted as the southernmost exposures of the Lemhi subbasin of the Mesoproterozoic Belt Supergroup.

The upper Wildhorse gneiss includes ca. 695 Ma intrusive orthogneiss that is coeval with Neoproterozoic rift-related volcanic or intrusive rocks near Pocatello, House Mountain, and Edwardsburg, Idaho. This Cryogenian meta-intrusive rock is the likely source of the 650–710 Ma detrital-zircon population in the Big Lost River that drains the core complex. Initial ϵ_{Hf} values from 675 Ma zircons are between 3.4 and –2.4, suggesting the granitoids had a mixed source in both continental crust and juvenile mantle.

INTRODUCTION

The Pioneer Mountains core complex (PMCC) contains the Wildhorse gneiss, the largest exposure of Precambrian basement in central Idaho. The protolith ages of these metamorphic rocks are important because they place constraints on the boundary between the Archean Grouse Creek block and Paleoproterozoic metamorphic basement to the north within the Great Falls tectonic zone and Selway terrane (Fig. 1). Further, some gneisses in the Pioneer

Mountains may be metamorphosed Belt Supergroup and can thus define the south end of the Belt Basin. Finally, detrital-zircon studies of Big Lost River alluvium demonstrate the presence of a ca. 650–710 Ma population, which may be derived from Cryogenian intrusive rocks in the Wildhorse complex. The Wildhorse gneiss is therefore an important and unique window into the age and tectonic affinity of the Precambrian crust of central Idaho.

Our goals were to investigate the age and correlation of protoliths in the gneiss complex of Wildhorse Creek, the structurally lowest lithodeme in the Pioneer Mountains, south-central Idaho (Dover, 1969, 1981, 1983; O'Neill and Pavlis, 1988). Prior to this study, the only available radiometric date from the Wildhorse complex was a ca. 2.0 Ga Rb-Sr whole-rock age reported by Dover (1983). The exposures were recognized as part of the Pioneer Mountains metamorphic core complex by Wust (1986). Much of the deformation and magmatism within the PMCC has been interpreted as Eocene (Vogl et al., 2012).

In this paper, we present U-Pb zircon data for 15 rock samples, representing a complete structural section of the Wildhorse gneiss, and one sample of Wildhorse Creek alluvium. These data help to address three primary issues: (1) whether the Wildhorse gneiss in the PMCC is part of the Archean Grouse Creek basement block (Fig. 1) (Gaschnig et al., 2013); (2) the location of the southern extent of the Mesoproterozoic Belt Supergroup, which is extensively exposed to the north and east (Fig. 1; Link et al., 2007); and (3) the origin of the population of anomalous 650–710 Ma zircon grains found in Big Lost River alluvium (Link et al., 2005).

■ PRECAMBRIAN BASEMENT IN THE NORTHERN ROCKIES

North of the Snake River Plain, Precambrian metamorphic basement is exposed in the Pioneer Mountains and in isolated areas within the Atlanta lobe of the Idaho batholith to the southwest (Fig. 1 inset) (O'Neill and Pavlis, 1988; Mueller et al., 2002; Foster et al., 2006; Gaschnig et al., 2013; Ma et al., 2016). Proterozoic metamorphic rocks also occur in the Beaverhead Mountains along the Idaho-Montana border where several exposures have U-Pb zircon crystallization ages ca. 2.45 Ga (Kellogg et al., 2003). Immediately to the south of the Coyote Creek quadrangle (Fig. 1 inset), the gneiss of Bloody Dick Creek contains a significant population (50%) of ca. 1.88 Ga zircons (Sherwin et al., 2016).

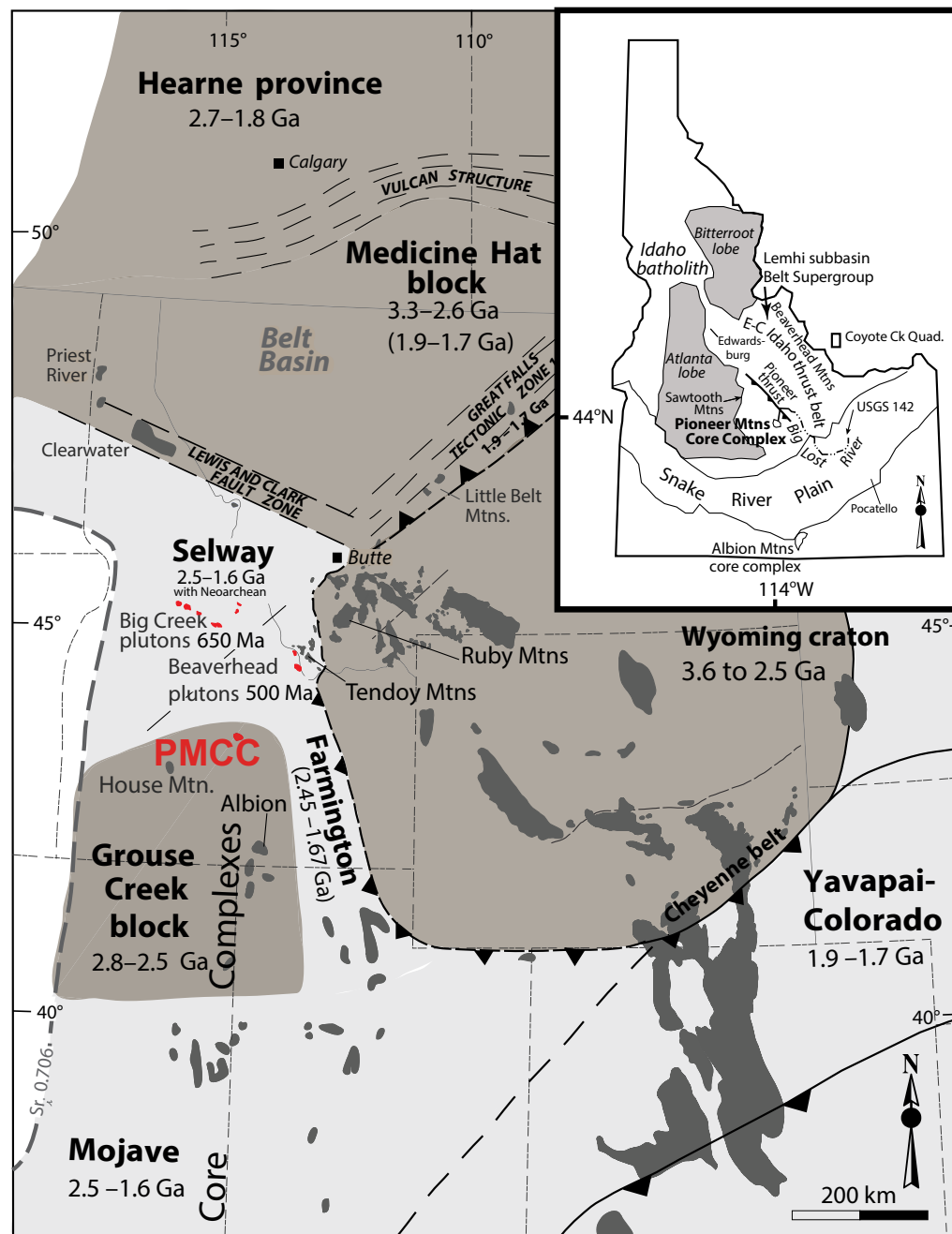


Figure 1. General tectonic map of western Laurentia showing ages of terranes and geographic areas mentioned in text (after Foster et al., 2006, and Mueller et al., 2011). General trend of belt of metamorphic core complexes is shown. Dark areas are Paleoproterozoic and older metamorphic rock exposures. Belt Basin contains Mesoproterozoic metasedimentary rock. The Pioneer Mountain core complex (PMCC, shown in red) and House Mountain exposures are labeled. Big Creek (650 Ma) and Beaverhead (500 Ma) plutons in east-central Idaho (Lund et al., 2010) are shown in red. Clump of exposures in northwestern Utah and adjacent Idaho is the Albion-Raft River core complex. Inset map: Geographic map of Idaho showing features and geologic units mentioned in text. The Big Lost River drains from the Pioneer Mountains to the Snake River Plain and transports distinctive 675 Ma zircon grains. Location of U.S. Geological Survey (USGS) Drill Hole 142 is shown.

Mueller et al. (2016) report on two samples from the gneiss of Bloody Dick Creek. Sample BDC-2 has a primary age of 1904 ± 13 Ma and sample BDC-6 has a primary age of 1799 ± 7 Ma. To the north in Montana, the Selway terrane and Great Falls tectonic zone (Fig. 1; O'Neill and Lopez, 1985) contain Paleoproterozoic juvenile crust (1.7–1.86 Ga) with older fragments at 2.2–2.6 Ga (Foster et al., 2006, 2012; Gifford et al., 2014). Alcock and Muller (2012) and Alcock et al. (2013) identify Paleoproterozoic strata (Montana metasedimentary terrane) in what had been considered Archean rocks of the Wyoming Province in the Ruby Range of southwest Montana (Fig. 1). The northern Bitterroot lobe of the Idaho batholith intrudes Paleoproterozoic 1.6–1.8 Ga primitive arc-like rocks (Toth and Stacey, 1992; Mueller et al., 1996; Foster and Fanning, 1997).

In the Albion Mountains to the south of the Neogene Snake River Plain (Fig. 1), the basement comprises the Neoproterozoic Grouse Creek complex (2.5–2.6 Ga; see Egger et al., 2003; Strickland et al., 2011). Xenoliths of felsic gneiss in Snake River Plain basalt lavas contain zircons with ages of 2.5–3.2 Ga (Lee-man et al., 1985; Wolf et al., 2005). East of the exposed Grouse Creek block, the Farmington complex contains gneisses with earliest Paleoproterozoic ages of ca. 2.45 Ga (Foster et al., 2006; Shervais, 2006; Mueller et al., 2011).

The intracratonic Belt basin north and east of the Pioneer Mountains contains the Belt Supergroup, principally quartzose and locally feldspathic strata that were deposited between ca. 1470 and ca. 1390 Ma (Harrison et al., 1974; Ruppel, 1975; Winston and Link, 1993) (Fig. 1). Comparable sequences in Idaho were deposited in the Lemhi subbasin (Fig. 1 inset). The rocks of the Belt basin and the Lemhi subbasin share broad stratigraphic relations, detrital-zircon age populations, have overlapping depositional age constraints, and cannot be structurally separated (Winston et al., 1999; Link et al., 2007, 2016; Stewart et al., 2010; Burmester et al., 2016). The southern extent of the Belt Supergroup is currently unknown.

■ PIONEER MOUNTAINS

The Pioneer metamorphic core complex (Wust, 1986; O'Neill and Pavlis, 1988; Silverberg, 1990; Worl et al., 1995; Vogl et al., 2012, 2014; McFadden et al., 2015) is part of the belt of Cordilleran metamorphic core complexes (Fig. 1) that formed during Cenozoic postorogenic extension in the hinterland of the Sevier orogenic belt. Precambrian and lower Paleozoic rocks are exposed in the footwall of the Wildhorse detachment fault (Dover, 1981, 1983; Wust, 1986). Within that footwall, Umpleby et al. (1930) recognized the Wildhorse gneiss in the structurally lowest exposures. Dover (1983) divided the gneiss complex of Wildhorse Creek into a lower (quartzitic) gneiss, a middle (felsic) orthogneiss, a mafic gneiss, and an upper (quartzitic) gneiss. The ages for all those units were designated as Paleoproterozoic on the basis of preliminary Rb-Sr whole-rock dating. A revised geologic map of the Wildhorse gneiss that incorporates our recent U-Pb zircon age data is given as Figure 2.

The footwall of the PMCC contains a NNW-trending, doubly plunging anti-form (Wildhorse dome) that is cored by the Wildhorse complex (Fig. 2). Above

the gneiss, on the southwest flank of the Wildhorse dome, is a broadly concordant granodiorite sheet with a U-Pb zircon crystallization age of 48.6 ± 0.4 Ma (Vogl et al., 2012). On the east side of the dome is a large expanse of this Eocene granodiorite, locally termed the Pioneer Intrusive Suite (Fig. 2).

The PMCC developed in the Eocene, with extension beginning before ca. 49 Ma and continuing (perhaps episodically) through the Late Eocene. The Wildhorse gneiss underwent high-grade metamorphism and partial melting during the early stages of extension, during and/or before emplacement of voluminous granitoids at ca. 47–50 Ma (Vogl et al., 2012). The base of the middle structural plate of the Wildhorse gneiss (Fig. 2, cross section) underwent metamorphism at depths of ~11–15 km as a result of emplacement of the 48–49 Ma granodiorite sheet. Penetrative strain accompanied amphibolite-facies metamorphism throughout the Wildhorse gneiss and the basal middle plate (Vogl et al., 2012). The pervasive strain, metamorphism, melting, and widespread small-scale intrusions obscure the primary contact relationships between individual units within the basement exposures.

Structurally above the Eocene granodiorite is quartzite, marble, and schist of the middle structural plate of the PMCC. Along this boundary, Vogl et al. (2012) have identified significant structural omissions that predate intrusion of the granodiorite sheet. They suggested that the boundary was an extensional fault along which the granodiorite intruded (Fig. 2, cross section).

Ma et al. (2016) examined zircons in Paleozoic wall rocks of the Idaho batholith in the Sawtooth Mountains (location shown in Fig. 1 inset). Their samples all contain Mesoproterozoic (Grenville-age) zircons 1200–1000 Ma and are therefore younger than any of the Wildhorse gneiss complex. These rocks likely are of the same age as metaquartzites and calc-silicate schists in the middle structural plate within the Pioneer Mountains, structurally above the Wildhorse gneiss (unit OCZs on Fig. 2).

The upper plate of the core complex, above the Wildhorse detachment fault, contains Paleozoic sedimentary rocks of the central Idaho thrust belt including the Devonian Milligen Formation and Pennsylvanian and Permian Sun Valley Group (Mahoney et al., 1991; Link et al., 1995, 2014). To the north and east of the PMCC and the Pioneer thrust fault (Fig. 1 inset), upper-plate strata belong to the Lower Mississippian Copper Basin Group (Link et al., 1996; Beranek et al., 2016).

■ METHODS

Durk (2007) conducted field mapping and sampling of the headwaters of Wildhorse Creek. Cameron (2010) mapped and sampled a section of the Wildhorse gneiss on the southwest flank of the dome. To complement this Idaho State University senior thesis work, Vogl and Foster conducted reconnaissance sampling in 2013.

Zircon grains from Wildhorse Creek alluvium and Wildhorse complex orthogneiss and paragneiss were handpicked from heavy-mineral concentrates, placed onto double-sided tape, together with either Duluth Gabbro (FC1) or

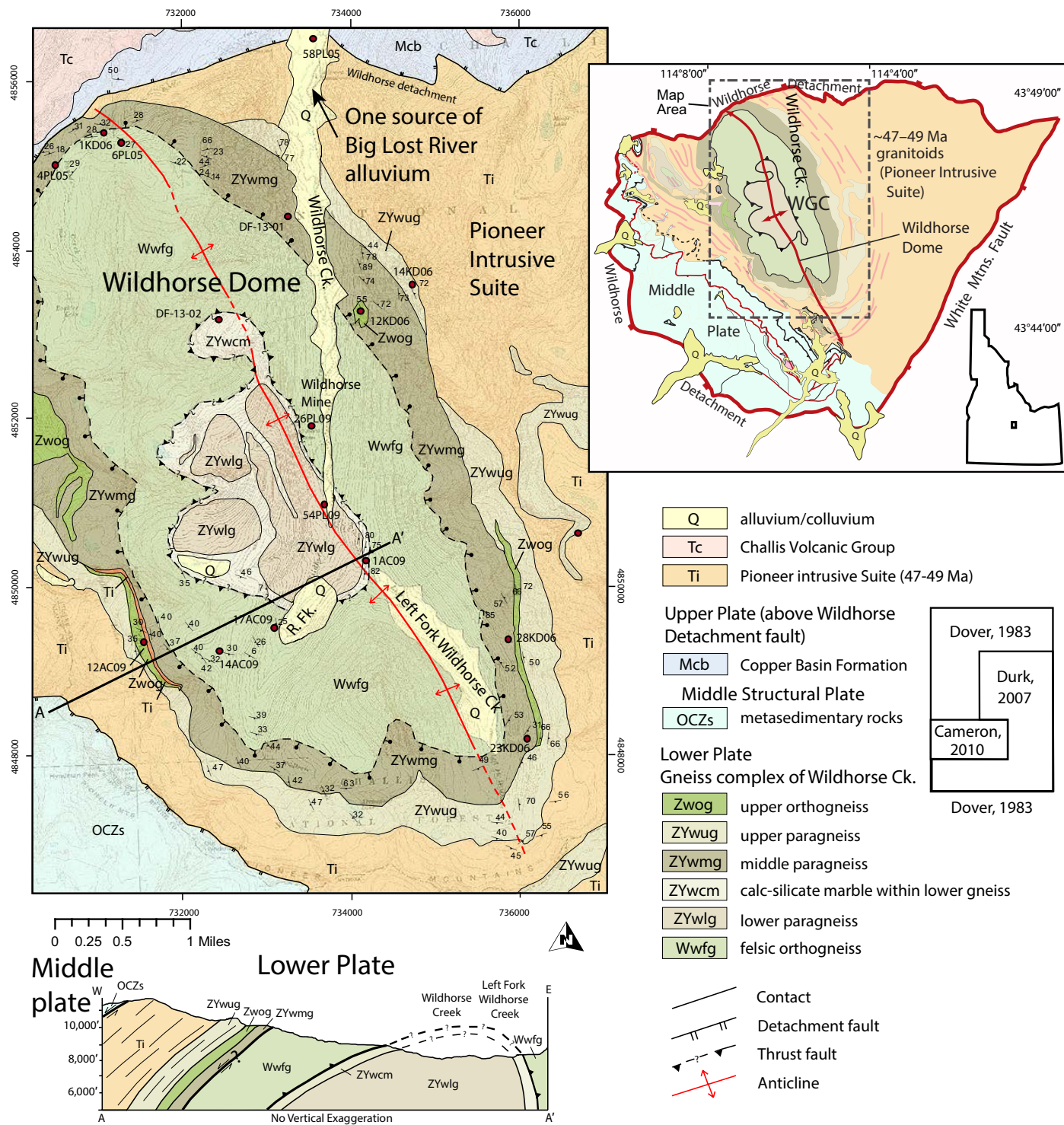


Figure 2. Geologic map and cross section of the gneiss complex of Wildhorse Creek, showing locations of samples discussed in this paper. Inset map shows regional context of Pioneer Mountain core complex (PMCC). Cross section shows structural arrangement of map units, and serves also as a stratigraphic diagram. WGC—Wildhorse Gneiss Complex.

Table 1. Link of Pioneer Mtns. ID

Table	Plot on Fig. 4	Sample	Easting	Northing	Elev. Ft.	Notes
1A	Fig. 4B	DF-13-01	114 0281W	43 783N	7811	Wildhorse, CK Alluvium
1B	Fig. 4B	DF-13-02	114 0281W	43 783N	7811	CK by Wildhorse Mine
1C	Fig. 4B	DF-13-03	114 0279W	43 782N	7800	Quartzite from lower paragneiss
1D	Fig. 4B	DF-13-04	114 0280W	43 782N	7800	CK by Wildhorse Mine
1E	Fig. 4B	DF-13-05	114 0280W	43 782N	7800	1 m white quartzite, L. Fk Wildhorse Cr.
1F	Fig. 4B	DF-13-06	114 0281W	43 779N	8161	Interbedded with marble
1G	Fig. 4B	DF-13-07	114 0280W	43 812N	8771	Felsic gneiss south of road in abandoned rift
1H	Fig. 4B	DF-13-08	114 0280W	43 812N	8771	metre-scale, medium to large grain size
1I	Fig. 4B	DF-13-09	114 0280W	43 815N	8751	mostly amber, some clear
1J	Fig. 4B	DF-13-10	114 0280W	43 815N	8751	metre-scale, medium to large grain size
1K	Fig. 4B	DF-13-11	114 0280W	43 815N	8751	metre-scale, medium to large grain size
1L	Fig. 4B	DF-13-12	114 0280W	43 815N	8751	metre-scale, medium to large grain size
1M	Fig. 4B	DF-13-13	114 0280W	43 815N	8751	metre-scale, medium to large grain size
1N	Fig. 4B	DF-13-14	114 0280W	43 815N	8751	metre-scale, medium to large grain size
1O	Fig. 4B	DF-13-15	114 0280W	43 815N	8751	metre-scale, medium to large grain size
1P	Fig. 4B	DF-13-16	114 0280W	43 815N	8751	metre-scale, medium to large grain size
1Q	Fig. 4B	DF-13-17	114 0280W	43 815N	8751	metre-scale, medium to large grain size
1R	Fig. 4B	DF-13-18	114 0280W	43 815N	8751	metre-scale, medium to large grain size
1S	Fig. 4B	DF-13-19	114 0280W	43 815N	8751	metre-scale, medium to large grain size
1T	Fig. 4B	DF-13-20	114 0280W	43 815N	8751	metre-scale, medium to large grain size
1U	Fig. 4B	DF-13-21	114 0280W	43 815N	8751	metre-scale, medium to large grain size
1V	Fig. 4B	DF-13-22	114 0280W	43 815N	8751	metre-scale, medium to large grain size
1W	Fig. 4B	DF-13-23	114 0280W	43 815N	8751	metre-scale, medium to large grain size
1X	Fig. 4B	DF-13-24	114 0280W	43 815N	8751	metre-scale, medium to large grain size
1Y	Fig. 4B	DF-13-25	114 0280W	43 815N	8751	metre-scale, medium to large grain size
1Z	Fig. 4B	DF-13-26	114 0280W	43 815N	8751	metre-scale, medium to large grain size
2A	Fig. 4B	DF-13-27	114 0280W	43 815N	8751	metre-scale, medium to large grain size
2B	Fig. 4B	DF-13-28	114 0280W	43 815N	8751	metre-scale, medium to large grain size
2C	Fig. 4B	DF-13-29	114 0280W	43 815N	8751	metre-scale, medium to large grain size
2D	Fig. 4B	DF-13-30	114 0280W	43 815N	8751	metre-scale, medium to large grain size
2E	Fig. 4B	DF-13-31	114 0280W	43 815N	8751	metre-scale, medium to large grain size
2F	Fig. 4B	DF-13-32	114 0280W	43 815N	8751	metre-scale, medium to large grain size
2G	Fig. 4B	DF-13-33	114 0280W	43 815N	8751	metre-scale, medium to large grain size
2H	Fig. 4B	DF-13-34	114 0280W	43 815N	8751	metre-scale, medium to large grain size
2I	Fig. 4B	DF-13-35	114 0280W	43 815N	8751	metre-scale, medium to large grain size
2J	Fig. 4B	DF-13-36	114 0280W	43 815N	8751	metre-scale, medium to large grain size
2K	Fig. 4B	DF-13-37	114 0280W	43 815N	8751	metre-scale, medium to large grain size
2L	Fig. 4B	DF-13-38	114 0280W	43 815N	8751	metre-scale, medium to large grain size
2M	Fig. 4B	DF-13-39	114 0280W	43 815N	8751	metre-scale, medium to large grain size
2N	Fig. 4B	DF-13-40	114 0280W	43 815N	8751	metre-scale, medium to large grain size
2O	Fig. 4B	DF-13-41	114 0280W	43 815N	8751	metre-scale, medium to large grain size
2P	Fig. 4B	DF-13-42	114 0280W	43 815N	8751	metre-scale, medium to large grain size
2Q	Fig. 4B	DF-13-43	114 0280W	43 815N	8751	metre-scale, medium to large grain size
2R	Fig. 4B	DF-13-44	114 0280W	43 815N	8751	metre-scale, medium to large grain size
2S	Fig. 4B	DF-13-45	114 0280W	43 815N	8751	metre-scale, medium to large grain size
2T	Fig. 4B	DF-13-46	114 0280W	43 815N	8751	metre-scale, medium to large grain size
2U	Fig. 4B	DF-13-47	114 0280W	43 815N	8751	metre-scale, medium to large grain size
2V	Fig. 4B	DF-13-48	114 0280W	43 815N	8751	metre-scale, medium to large grain size
2W	Fig. 4B	DF-13-49	114 0280W	43 815N	8751	metre-scale, medium to large grain size
2X	Fig. 4B	DF-13-50	114 0280W	43 815N	8751	metre-scale, medium to large grain size
2Y	Fig. 4B	DF-13-51	114 0280W	43 815N	8751	metre-scale, medium to large grain size
2Z	Fig. 4B	DF-13-52	114 0280W	43 815N	8751	metre-scale, medium to large grain size

¹Supplemental Table S1. GPS locations of samples presented in this study. Table where data are shown and figure numbers are indicated. Please visit <http://doi.org/10.1130/GES01418.S1> or the full-text article on www.gsapubs.org to view Table S1.

Table 2. Fig. 15. Summary of SHRIMP U-Pb data for sample 54PL09.

Grain #	U (ppm)	Pb (ppm)	Age (Ma)	σ (Ma)	Notes
1	1.1	0.1	3250	10	
2	1.2	0.1	3250	10	
3	1.3	0.1	3250	10	
4	1.4	0.1	3250	10	
5	1.5	0.1	3250	10	
6	1.6	0.1	3250	10	
7	1.7	0.1	3250	10	
8	1.8	0.1	3250	10	
9	1.9	0.1	3250	10	
10	2.0	0.1	3250	10	
11	2.1	0.1	3250	10	
12	2.2	0.1	3250	10	
13	2.3	0.1	3250	10	
14	2.4	0.1	3250	10	
15	2.5	0.1	3250	10	
16	2.6	0.1	3250	10	
17	2.7	0.1	3250	10	
18	2.8	0.1	3250	10	
19	2.9	0.1	3250	10	
20	3.0	0.1	3250	10	
21	3.1	0.1	3250	10	
22	3.2	0.1	3250	10	
23	3.3	0.1	3250	10	
24	3.4	0.1	3250	10	
25	3.5	0.1	3250	10	
26	3.6	0.1	3250	10	
27	3.7	0.1	3250	10	
28	3.8	0.1	3250	10	
29	3.9	0.1	3250	10	
30	4.0	0.1	3250	10	
31	4.1	0.1	3250	10	
32	4.2	0.1	3250	10	
33	4.3	0.1	3250	10	
34	4.4	0.1	3250	10	
35	4.5	0.1	3250	10	
36	4.6	0.1	3250	10	
37	4.7	0.1	3250	10	
38	4.8	0.1	3250	10	
39	4.9	0.1	3250	10	
40	5.0	0.1	3250	10	
41	5.1	0.1	3250	10	
42	5.2	0.1	3250	10	
43	5.3	0.1	3250	10	
44	5.4	0.1	3250	10	
45	5.5	0.1	3250	10	
46	5.6	0.1	3250	10	
47	5.7	0.1	3250	10	
48	5.8	0.1	3250	10	
49	5.9	0.1	3250	10	
50	6.0	0.1	3250	10	

²Supplemental Table S2. U-Pb sensitive high-resolution ion microprobe (SHRIMP) data for the samples described in this paper. Please visit <http://doi.org/10.1130/GES01418.S2> or the full-text article on www.gsapubs.org to view Table S2.

Table 3. U-Pb sensitive high-resolution ion microprobe (SHRIMP) data for samples from Pioneer Mountains, Idaho.

Sample	Grain #	U (ppm)	Pb (ppm)	Age (Ma)	σ (Ma)	Notes
54PL09	1	1.1	0.1	3250	10	
	2	1.2	0.1	3250	10	
	3	1.3	0.1	3250	10	
	4	1.4	0.1	3250	10	
	5	1.5	0.1	3250	10	
	6	1.6	0.1	3250	10	
	7	1.7	0.1	3250	10	
	8	1.8	0.1	3250	10	
	9	1.9	0.1	3250	10	
	10	2.0	0.1	3250	10	
24KD06	1	1.1	0.1	3250	10	
	2	1.2	0.1	3250	10	
	3	1.3	0.1	3250	10	
	4	1.4	0.1	3250	10	
	5	1.5	0.1	3250	10	
	6	1.6	0.1	3250	10	
	7	1.7	0.1	3250	10	
	8	1.8	0.1	3250	10	
	9	1.9	0.1	3250	10	
	10	2.0	0.1	3250	10	
1AC09	1	1.1	0.1	3250	10	
	2	1.2	0.1	3250	10	
	3	1.3	0.1	3250	10	
	4	1.4	0.1	3250	10	
	5	1.5	0.1	3250	10	
	6	1.6	0.1	3250	10	
	7	1.7	0.1	3250	10	
	8	1.8	0.1	3250	10	
	9	1.9	0.1	3250	10	
	10	2.0	0.1	3250	10	

³Supplemental Table S3. U-Pb data for the samples run on laser ablation–multicollector–inductively coupled plasma mass spectrometry (LA-MC-ICPMS) at the University of Florida. Sample localities and figure in the paper are specified in Table S1. Please visit <http://doi.org/10.1130/GES01418.S3> or the full-text article on www.gsapubs.org to view Table S3.

Temora reference zircons, cast into epoxy disks and sectioned approximately in half, and polished. Transmitted- and reflected-light photomicrographs and cathodoluminescence (CL) images were made for all grains. Because the zircon grains from these gneissic samples have thin metamorphic rims, likely Eocene in age, for the purposes of this study, the areas analyzed were concentrated on the central areas that were considered to record the primary protolith history. The U-Pb analyses for 14 samples were carried out using sensitive high-resolution ion microprobe–reverse geometry (SHRIMP-RG and SHRIMP II) at the Research School of Earth Sciences, The Australian National University, Canberra, Australia, following procedures described in Williams (1998) and references therein. The data have been processed using the SQUID Excel macro of Ludwig (2000). Plots and age calculations were carried out using Isoplot/Ex, version 3.00 (Ludwig, 2003). A concordance filter of 20% was used for the paragneiss samples. GPS locations and sample descriptions are in Table S1¹. Data for samples run on the SHRIMP are shown in Table S2². Two other samples, DF-13-01 and DF-13-02, were dated by laser ablation–multicollector–inductively coupled mass spectrometry (LA-MC-ICPMS) at the University of Florida using methods similar to those described in Foster et al. (2012); data are given in Table S3³.

We ran Lu-Hf isotopes on selected 675 Ma detrital zircons from a subsurface sample of Big Lost River alluvium, using LA-MC-ICPMS at the Arizona Laserchron Laboratory, following the methods outlined in Cecil et al. (2011) and Gehrels and Pecha (2014). Data are in Table S4⁴. Hf isotopic values bear on the nature of the crust that was partially melted to produce the plutons in which the zircons crystallized (Kinny and Maas, 2003; Goodge and Vervoort, 2006; Bahlburg et al., 2011).

Table 4. Hf isotopic data for CM142-795, USGS Drill Hole 142, 795 ft deep.

Sample	¹⁷⁷ Hf/ ¹⁷⁹ Hf	¹⁷⁶ Hf/ ¹⁷⁷ Hf	Age (Ma)	σ (Ma)	Notes
LN142-795-01	0.282476	0.000000	3250	10	
LN142-795-02	0.282476	0.000000	3250	10	
LN142-795-03	0.282476	0.000000	3250	10	
LN142-795-04	0.282476	0.000000	3250	10	
LN142-795-05	0.282476	0.000000	3250	10	
LN142-795-06	0.282476	0.000000	3250	10	
LN142-795-07	0.282476	0.000000	3250	10	
LN142-795-08	0.282476	0.000000	3250	10	
LN142-795-09	0.282476	0.000000	3250	10	
LN142-795-10	0.282476	0.000000	3250	10	
LN142-795-11	0.282476	0.000000	3250	10	
LN142-795-12	0.282476	0.000000	3250	10	
LN142-795-13	0.282476	0.000000	3250	10	
LN142-795-14	0.282476	0.000000	3250	10	
LN142-795-15	0.282476	0.000000	3250	10	
LN142-795-16	0.282476	0.000000	3250	10	
LN142-795-17	0.282476	0.000000	3250	10	
LN142-795-18	0.282476	0.000000	3250	10	
LN142-795-19	0.282476	0.000000			

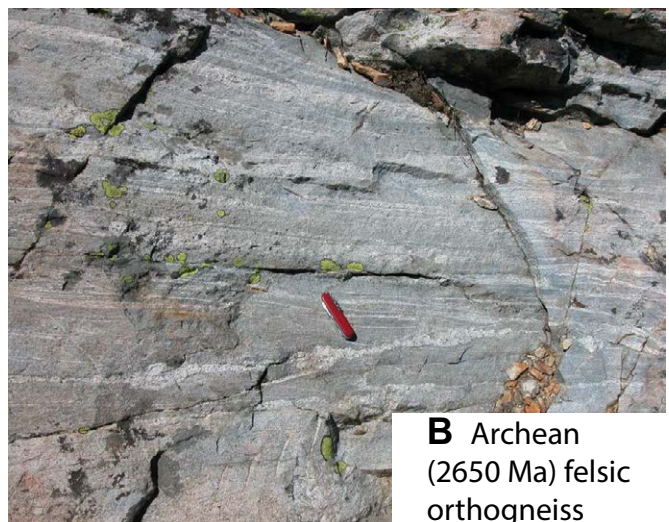
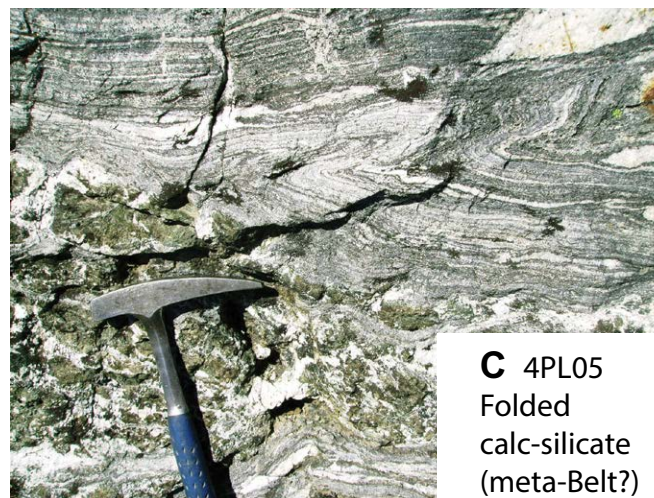
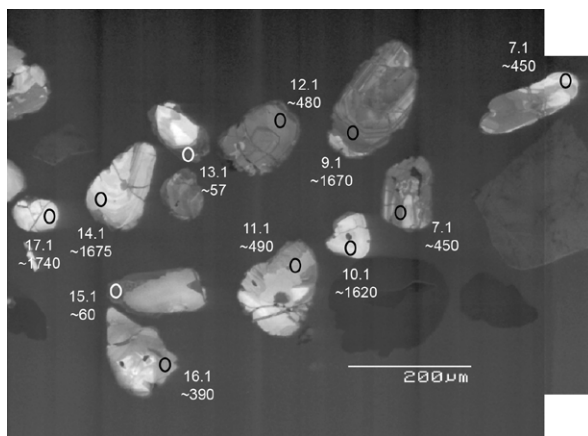


Figure 3. Field photographs of main lithologic units. (A) Quartzitic lower paragneiss, Wildhorse Creek (sample 26PL09). (B) Archean orthogneiss (sample 6PL05) east of Boulder Creek. (C) Folded calc-silicate gneiss from middle gneiss, interpreted as metamorphosed Belt Supergroup (sample 4PL05). (D) Neoproterozoic orthogneiss (sample 23KD06).

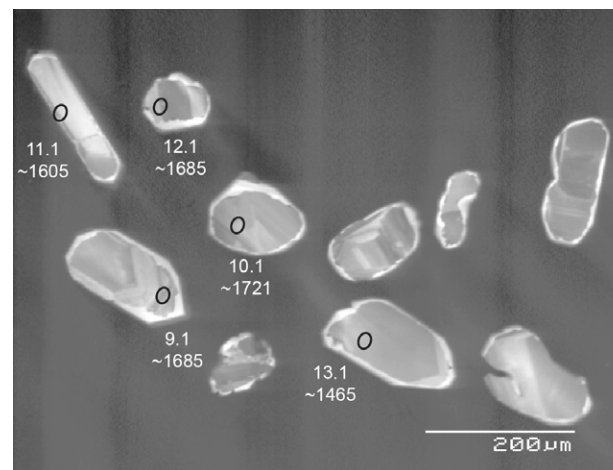
have been significantly modified since primary crystallization. The CL images (Fig. 4A) show that many are cracked and have irregular internal structures. For the 44 grains analyzed, there is a wide variety of apparent ages ranging from the Eocene (ca. 50 Ma) to Archean (ca. 2865 Ma) (Figs. 5F and 5G; Table S2B [see footnote 2]). There is a prominent Proterozoic grouping of 11 analyses that define a discordia trend with an upper intercept at 1710 ± 30 Ma (Fig. 5G) to a lower intercept at ca. 94 Ma. As expected, there are a number of areas of new zircon growth that relate to superimposed younger events, including those in the Eocene, and perhaps during the Ordovician.

Felsic Orthogneiss

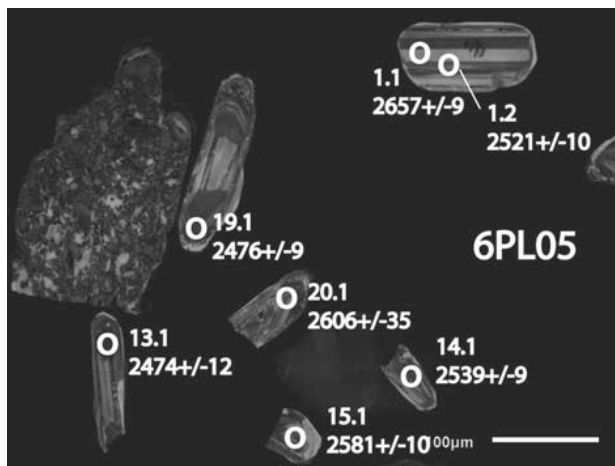
Felsic orthogneiss ~700 m thick overlies the lower paragneiss around the entire Wildhorse dome (map unit Wwfg, Middle gneiss of Dover, 1983). The rock is light-gray to white, equigranular, fine to medium grained, and varies from biotite quartz monzonite to trondhjemite gneiss. The lower contact of this paragneiss is sharp but not well exposed. We follow Cameron (2010) and interpret the contact as a thrust fault. The felsic orthogneiss forms the high walls of many of the cirques in the area.



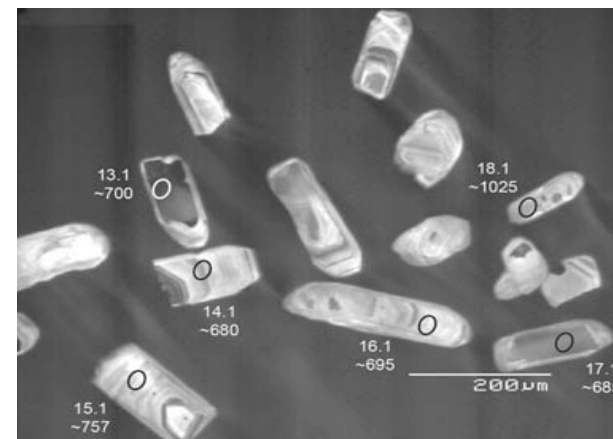
A 1AC09 lower paragneiss



C 14KD06 upper paragneiss



B 6PL05 Neoproterozoic orthogneiss



D 23KD06 upper orthogneiss (Neoproterozoic)

Figure 4. Cathodoluminescence images. (A) Cathodoluminescence (CL) images for quartzose paragneiss sample 1AC09 from the lowest exposed rocks in the Wildhorse gneiss. The grains are rounded, and originally detrital, but the zircon age distribution is complex. Several detrital grains are 1740–1620 Ma, but Paleozoic and Eocene zircons are also present. These grains crystallized during a complex metamorphic and intrusive history. (B) CL image for sample 6PL05, a 2.6 Ga Neoproterozoic felsic orthogneiss (photograph in Fig. 3B), structurally low in the Wildhorse gneiss. This rock unit is correlated with the Neoproterozoic meta-intrusive rocks of the Grouse Creek block. (C) CL image for sample 14KD06, a Mesoproterozoic (or younger) quartzitic paragneiss interpreted to be metamorphosed Belt Supergroup. Zircons are rounded (detrital), and have both zoned magmatic and diffuse metamorphic, eroded cores. All <10% discordant grains are 1760–1490 Ma. Light-colored rims are likely Eocene. (D) CL image for sample 28KD06, Neoproterozoic orthogneiss (Zog) (see photograph in Fig. 3D). All euhedral zircons have magmatic zoning, and are ca. 700 Ma.

Zircons from four samples were dated from the north and southwest flanks of the Wildhorse dome (Fig. 6; samples 6PL05, 1KD06, 14AC09, and 17AC09; Tables S2E–S2H [see footnote 2]); a field photograph is given in Figure 3B with the Wetherill concordia plots given in Figure 6. Magmatic zircon grains in the felsic orthogneiss are clear, elongate prismatic, euhedral to subhedral, with a maximum size of ~275 microns (Fig. 4B). The larger zircons have well-defined oscillatory CL zoning. Most of the grains have diffuse central areas with a thin rim, and some have metamict cores.

The U-Pb data from all four samples define simple discordia regression arrays with upper intercept ages ranging from ca. 2595 Ma to ca. 2670 Ma (Fig. 6). We interpret the crystallization of this orthogneiss to be between 2.60 Ga to 2.65 Ga. The lower concordia intercepts for the regression lines range from ca. 100 to ca. 55 Ma, consistent with variable radiogenic lead loss during Eocene magmatism and metamorphism. The elevated U and lower Th/U ratios in some rims suggest that they are due to Eocene partial melting.

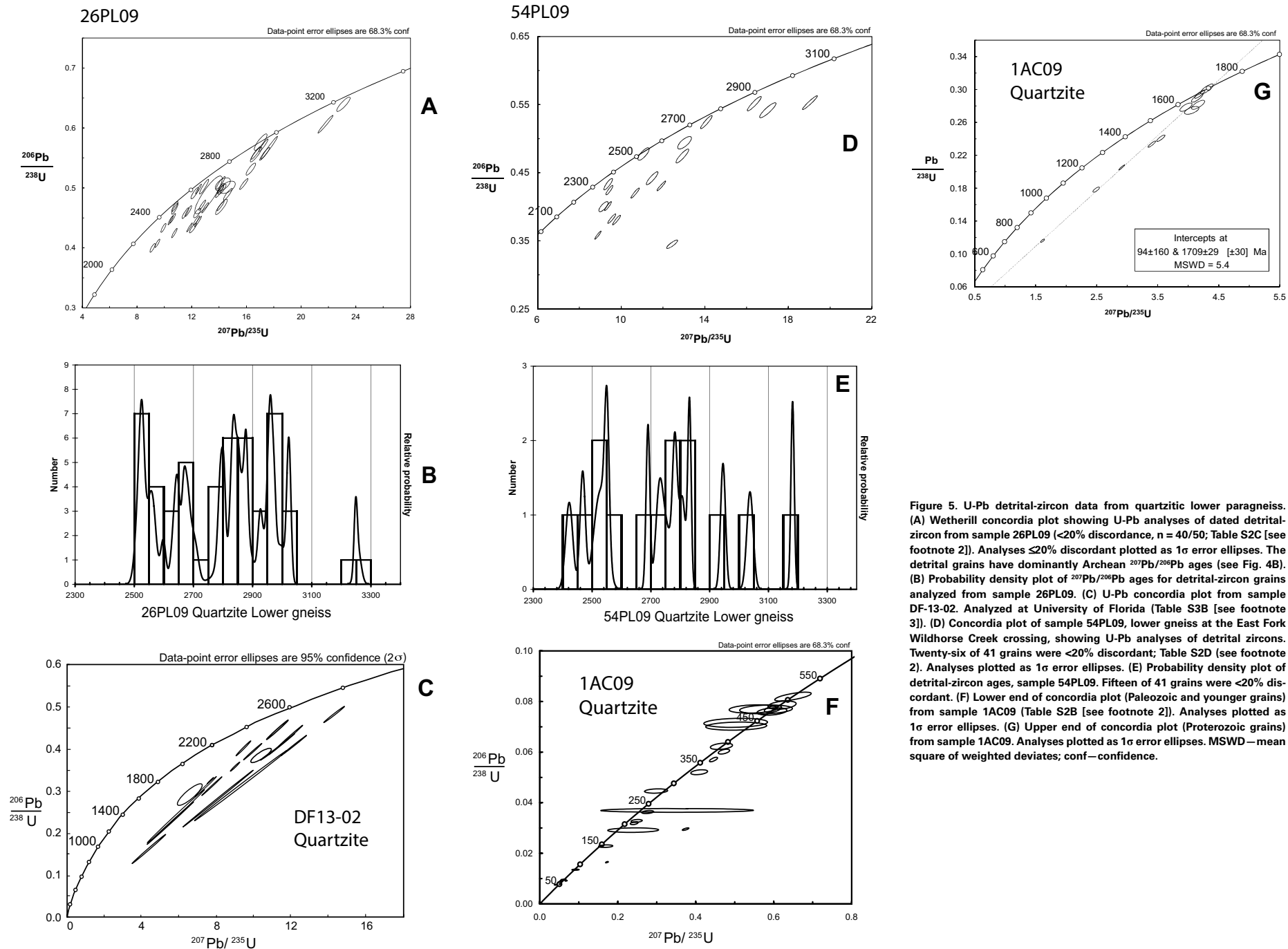


Figure 5. U-Pb detrital-zircon data from quartzitic lower paragneiss. (A) Wetherill concordia plot showing U-Pb analyses of dated detrital-zircon from sample 26PL09 (<20% discordance, n = 40/50; Table S2C [see footnote 2]). Analyses ≤20% discordant plotted as 1σ error ellipses. The detrital grains have dominantly Archean ²⁰⁷Pb/²⁰⁶Pb ages (see Fig. 4B). (B) Probability density plot of ²⁰⁷Pb/²⁰⁶Pb ages for detrital-zircon grains analyzed from sample 26PL09. (C) U-Pb concordia plot from sample DF-13-02. Analyzed at University of Florida (Table S3B [see footnote 3]). (D) Concordia plot of sample 54PL09, lower gneiss at the East Fork Wildhorse Creek crossing, showing U-Pb analyses of detrital zircons. Twenty-six of 41 grains were <20% discordant; Table S2D (see footnote 2). Analyses plotted as 1σ error ellipses. (E) Probability density plot of detrital-zircon ages, sample 54PL09. Fifteen of 41 grains were <20% discordant. (F) Lower end of concordia plot (Paleozoic and younger grains) from sample 1AC09 (Table S2B [see footnote 2]). Analyses plotted as 1σ error ellipses. (G) Upper end of concordia plot (Proterozoic grains) from sample 1AC09. Analyses plotted as 1σ error ellipses. MSWD—mean square of weighted deviates; conf—confidence.

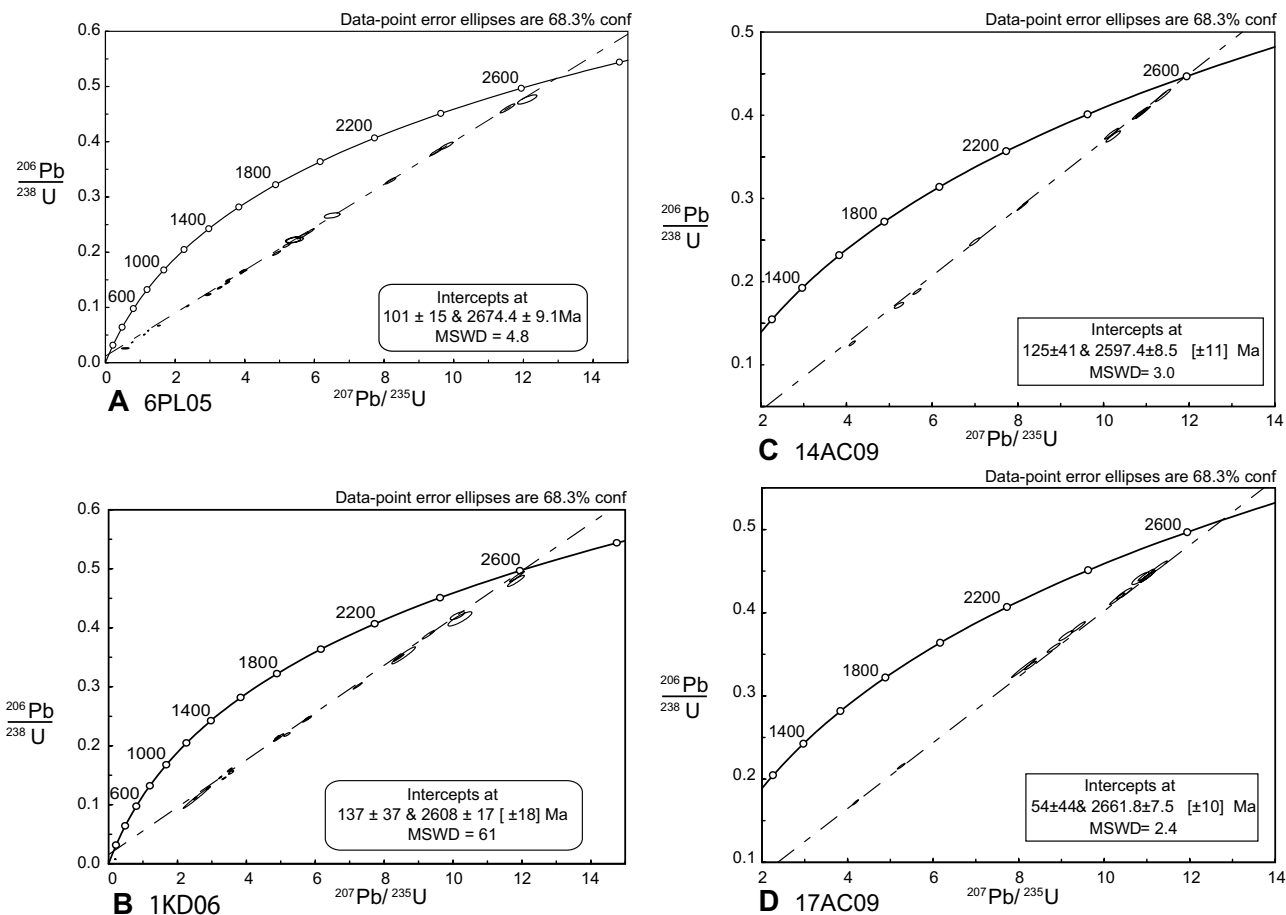


Figure 6. U-Pb data from felsic orthogneiss. (A) U-Pb concordia plot from felsic gneiss east of Boulder Creek (sample 6PL05; Table S2E [see footnote 2]). Photo in Figure 4B. Upper intercept age of 2674 ± 9 Ma. Analyses plotted as 1σ error ellipses. (B) U-Pb concordia plot from felsic gneiss (sample 1KD06; Table S2F [see footnote 2]). Analyses plotted as 1σ error ellipses. (C) U-Pb concordia plot from felsic gneiss (sample 14AC09; Table S2G [see footnote 2]). Upper intercept age of 2597 ± 8.5 Ma. Analyses plotted as 1σ error ellipses. (D) U-Pb concordia plot from felsic gneiss (sample 17AC09; Table S2H [see footnote 2]). Upper intercept age of 2661 ± 7.5 Ma. Analyses plotted as 1σ error ellipses. MSWD—mean square of weighted deviates; conf—confidence.

Middle Paragneiss

The felsic orthogneiss is overlain across a sheared zone or a sharp contact by a heterogeneous package of metasedimentary rocks, which we refer to as the middle paragneiss (map unit XYwmg; Mafic gneiss of Dover, 1983). This unit is dominated by fine- to medium- grained, equigranular, thinly layered metapsammitic paragneiss that is interlayered with quartzite gneiss and contains several intervals of diopside-bearing calc-silicate rock (Fig. 3C). The unit contains locally abundant amphibolite that cuts the calc-silicate. The amphibolite is commonly isoclinally folded and boudinaged. Overall, this unit is highly strained as indicated by the folds, boudins of Eocene leucogranite, and por-

phyroclastic quartz-feldspar aggregates. The structural thickness of this unit is ~500–700 m.

Zircon age data from the middle paragneiss are shown in Figure 7. Detrital zircons were analyzed from a calc-silicate (4PL05) from the lower part of the middle paragneiss at the north end of the Wildhorse dome. The zircons are predominantly round and subround grains with a few that are euhedral in shape; overall they are considered to be detrital. Twenty-one of 29 grains analyzed record U-Pb ages that are less than 20% discordant (Fig. 7A and Table S2I [see footnote 2]). The ²⁰⁷Pb/²⁰⁶Pb ages of these low-discordance grains range from ca. 1800 Ma to ca. 1400 Ma, with one grain at ca. 2600 Ma (Fig. 7B). The morphology and age data suggest that the sandstone protolith was

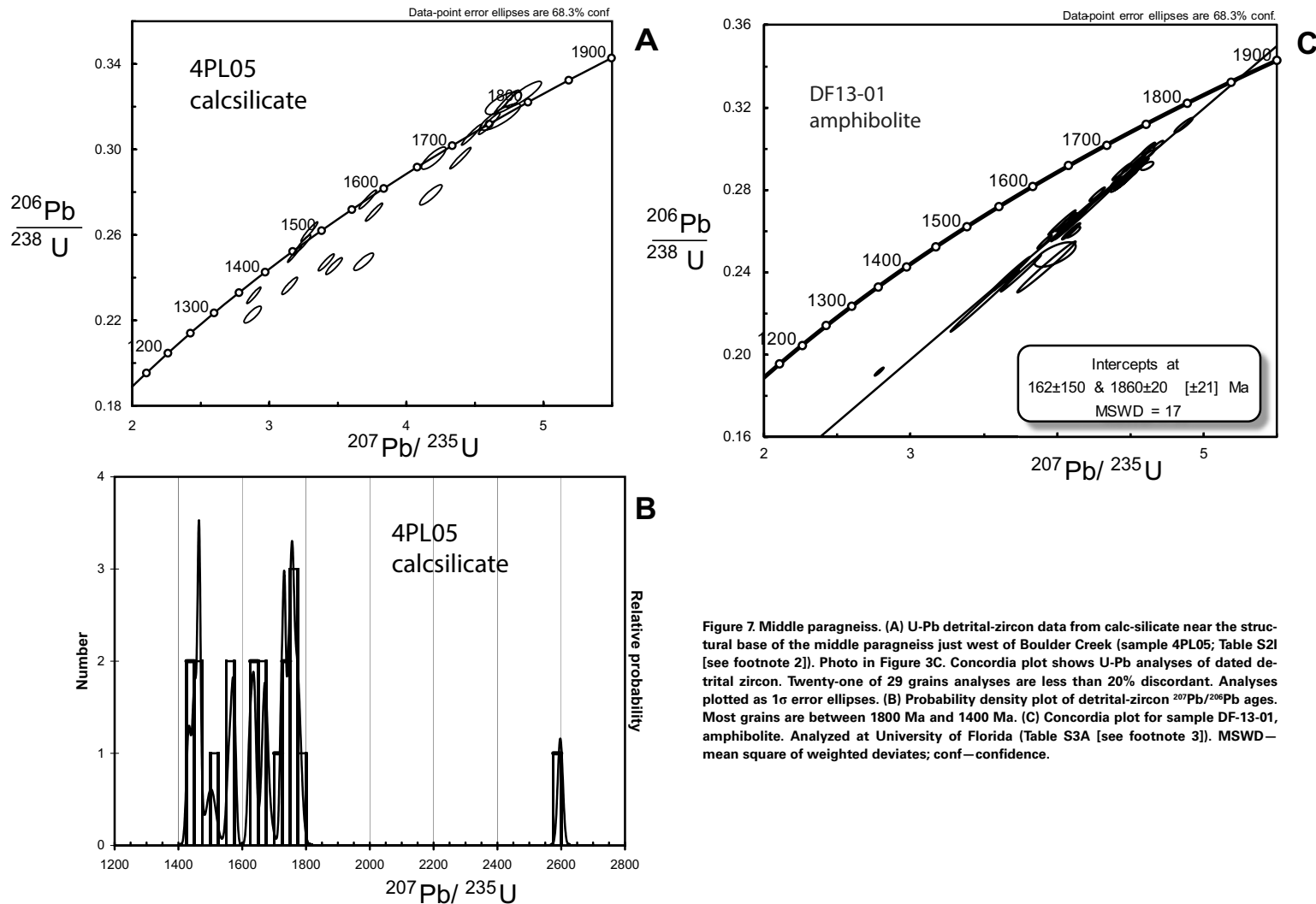


Figure 7. Middle paragneiss. (A) U-Pb detrital-zircon data from calc-silicate near the structural base of the middle paragneiss just west of Boulder Creek (sample 4PL05; Table S21 [see footnote 2]). Photo in Figure 3C. Concordia plot shows U-Pb analyses of dated detrital zircon. Twenty-one of 29 grains analyses are less than 20% discordant. Analyses plotted as 1σ error ellipses. (B) Probability density plot of detrital-zircon $^{207}\text{Pb}/^{235}\text{U}$ ages. Most grains are between 1800 Ma and 1400 Ma. (C) Concordia plot for sample DF-13-01, amphibolite. Analyzed at University of Florida (Table S3A [see footnote 3]). MSWD—mean square of weighted deviates; conf—confidence.

not deposited earlier than 1400 Ma and clearly could be much younger given the limited data set on this sample.

Sample DF-13-01 comes from a medium-grained lens of amphibolite within the middle part of the middle paragneiss unit where mafic boudins are abundant. The analyses scatter about a discordia trend with an upper intercept of 1860 ± 20 Ma (Fig. 7C; Table S3A [see footnote 3]). There are three possibilities for this age, all of which require the middle part of the middle paragneiss to be Paleoproterozoic or older. (1) If these boudins were basalt flows or synsedimentary sills, then this part of the section was deposited at ca. 1860 Ma. (2) If the zircon is metamorphic in origin, then the 1860 Ma zircon ages represent a minimum age of deposition of this part of the section. (3) If the boudins were originally mafic dikes, then the section must be older than 1860 Ma. Regardless of the interpretation, these data indicate that the entire middle paragneiss is not a Mesoproterozoic clastic package as previously suggested (Link et al., 2010) and that the protoliths of the lower exposures are younger than at least some of the structurally higher units.

mentary sills, then this part of the section was deposited at ca. 1860 Ma. (2) If the zircon is metamorphic in origin, then the 1860 Ma zircon ages represent a minimum age of deposition of this part of the section. (3) If the boudins were originally mafic dikes, then the section must be older than 1860 Ma. Regardless of the interpretation, these data indicate that the entire middle paragneiss is not a Mesoproterozoic clastic package as previously suggested (Link et al., 2010) and that the protoliths of the lower exposures are younger than at least some of the structurally higher units.

Upper Paragneiss

Above the biotite-rich middle paragneiss is the upper paragneiss (map unit ZYwug; Upper gneiss of Dover, 1983), comprising gneissose quartzite, quartzofeldspathic gneiss, minor calc-silicate, amphibolite, and fine- to coarse-grained augen gneiss. The unit is medium-gray to white, sometimes with a green hue, and medium fine to medium grained. The unit contains gneissose quartzite in the lower 10–30 m. Grains to granule size (>2 mm) are present east of Wildhorse Creek. The unit is intruded by Eocene and Neoproterozoic plutonic rocks in the upper part; the basal contact is irregular. On the southwest side of the Wildhorse dome, this unit is ~300 m thick (Cameron, 2010).

Data from detrital-zircon grains found in the gneissose quartzite are shown in Figure 8 (samples 14KD06 [Figs. 8A and 8B] and 24KD06 [Figs. 8C and 8D]; Tables S2J and S2K [see footnote 2]). The zircons are clear, some with a slight red hue, round to subround, ranging to elongate prismatic, subhedral grains that are up to 200 μm length, with an overall average size of around 100 μm . The CL images (see Fig. 4C) show little-zoned to unzoned central areas that dominate each sectioned grain, with a very narrow bright CL rim to most.

The $^{207}\text{Pb}/^{206}\text{Pb}$ ages for the detrital zircons from both samples are generally between ca. 1450 and ca. 1800 Ma with prominent peaks ca. 1650–1700 and ca. 1680 Ma, respectively (Fig. 8). Two older grains are recorded in sample 24KD06 (ca. 2080 Ma and 2850 Ma) and also two Neoproterozoic grains. These age dis-

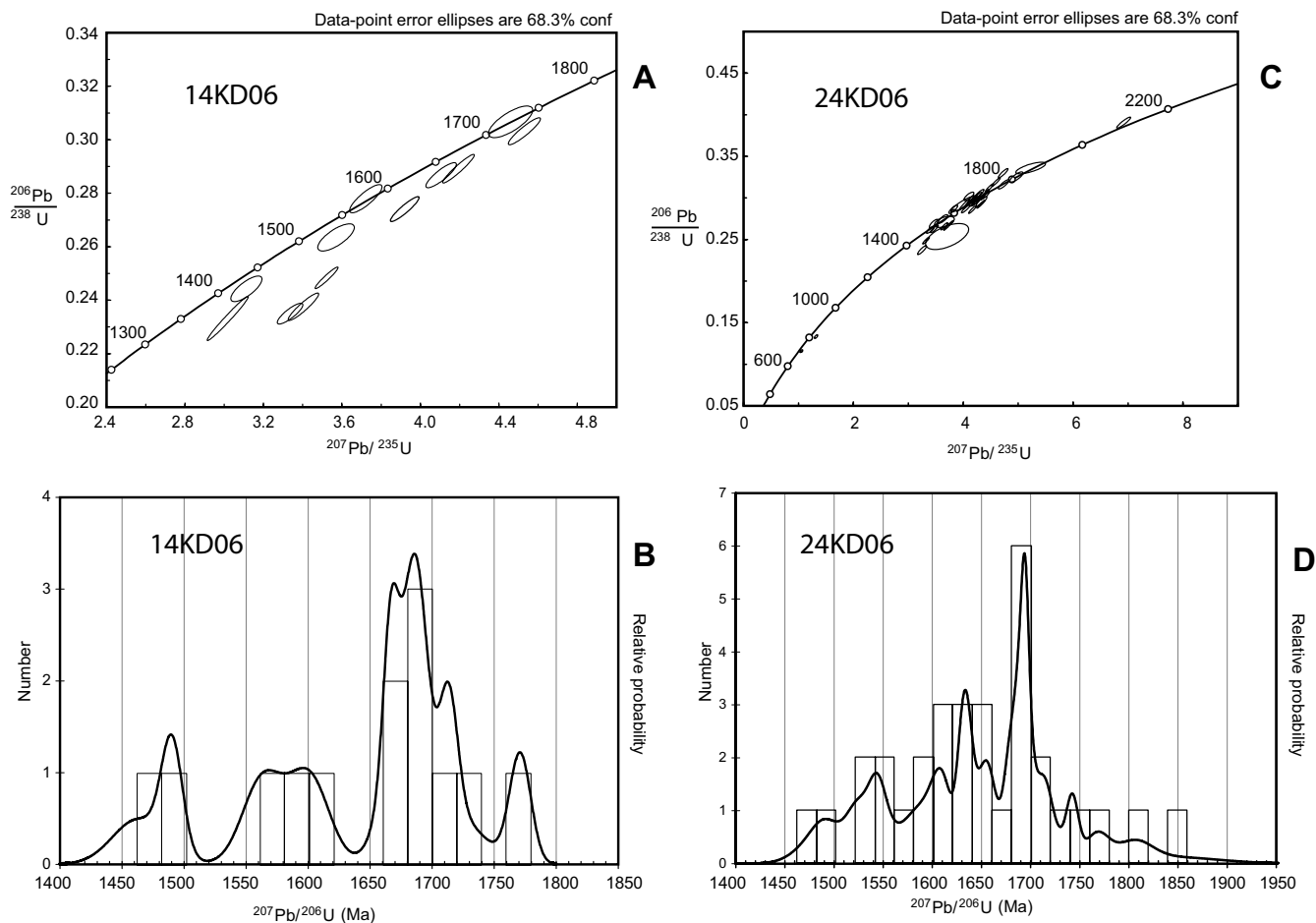


Figure 8. U-Pb detrital-zircon data from quartzite in upper paragneiss. (A) Sample 14KD06 concordia plot showing U-Pb analyses of dated detrital zircon, $n = 13$ (Table S2J [see footnote 2]). (B) Relative probability plot of detrital-zircon ages (sample 14KD06). Grains range from 1475 to 1775 Ma. (C) Sample 24KD06 concordia plot showing U-Pb analyses of dated detrital zircon (Table S2K [see footnote 2]). Thirty-four of 38 analyses <20% discordant are shown. Analyses plotted as 1 σ error ellipses. (D) Probability density plot of detrital-zircon $^{207}\text{Pb}/^{206}\text{Pb}$ ages (sample 24KD06). Grains range from 1475 to 1875 Ma. conf—confidence.

tributions are broadly similar to that of sample 4PL05 in the middle paragneiss but distinctly different than the solely Archean (>2500 Ma) and Paleoproterozoic (1700 Ma) detrital zircons in the four samples of the lower paragneiss. We interpret the detrital-zircon $^{207}\text{Pb}/^{206}\text{Pb}$ age to indicate deposition after ca. 1.45 Ga.

Upper Orthogneiss

The upper orthogneiss (map unit Zog; unit Xog of Dover, 1983) contains multiple white to orange medium- to coarse-grained bodies of biotite-hornblende quartz monzonite gneiss (Fig. 3D). At the map scale, these appear as concordant foliated lenses up to several tens of meters thick. However, in more detail on the outcrop scale, the contacts of these bodies cut lithologic layering in the middle and upper paragneisses, indicating an intrusive relationship. The unit has been injected by amphibolite dikes and sills that are now deformed.

Zircon age data from the orthogneiss are shown in Figure 9. Grains in samples 12KD06, 23KD06, and 28KD06 are clear, elongate prismatic, euhedral to subhedral, with a maximum size of ~500 microns, and an average size of 200 microns (CL images in Fig. 4D). The zircons in all three samples are interpreted to be simple zoned igneous crystals, but the subround nature of their exteriors implies postmagmatic processes have affected the grains.

Analyses from all three samples plot close to or within uncertainty of a Wetherill concordia, and in detail can be seen to form simple Pb-loss discordia trends, each with an upper intercept ca. 695 Ma (Figs. 9A–9C; Tables S2L–S2N [see footnote 2]; Durk, 2007). For sample 12KD06 (Fig. 9A), a linear regression has an upper concordia intercept at 692 ± 5 Ma (mean square of weighted deviates [MSWD] = 1.01, 20 analyses) with a lower intercept within uncertainty of the present day. Note that the analysis of grain 18 is discordant with an older $^{207}\text{Pb}/^{206}\text{Pb}$ age. A weighted mean for the 20 $^{207}\text{Pb}/^{206}\text{Pb}$ ages (Fig. 9D) gives 692 ± 5 Ma (MSWD = 0.98). The 20 zircon grains analyzed from 23KD06 form a tight, collinear array with 19 of the 20 analyses being $\leq 10\%$ discordant. Due to the limited amount of tightly clustered data, a regression line fitted to all 20 analyses is not precisely defined, with an upper intercept of 697 ± 9 Ma (MSWD = 1.05; Fig. 9B). A weighted mean for the $^{207}\text{Pb}/^{206}\text{Pb}$ ages gives 696 ± 8 Ma (MSWD = 1.07, 20 analyses) (Fig. 9E). As with the other two samples, the analyses from 28KD06 (Fig. 9C) form a linear regression on a Wetherill concordia plot with upper intercept at 696 ± 8 Ma (MSWD = 0.74). The lower intercept at ca. 220 Ma implies that the discordance arises, at least in part, from Mesozoic radiogenic Pb loss. The weighted-mean $^{207}\text{Pb}/^{206}\text{Pb}$ age therefore has some scatter (MSWD = 1.3) ca. 693 ± 7 Ma (Fig. 9F). This correspondence in the weighted mean of upper-intercept ages from all three samples, within two sigma error, leads to the conclusion that the crystallization age of the orthogneiss is ca. 695 Ma.

Wildhorse Creek Alluvium

The U-Pb data for the Neoproterozoic orthogneiss, and the discordance arrays, are almost identical with that for the anomalous, or “ghost” Neoproterozoic grains with 650–710 Ma ages found in Wildhorse Creek (Fig. 10;

Link et al., 2005; Hodges et al., 2009). The presence of 10% populations of these grains in Big Lost River alluvium suggested that the protolith must be present in the Pioneer Mountains. We now know that the source of these anomalous ages is the 695 Ma Neoproterozoic upper orthogneiss. Plutons of this general age are significant because they are interpreted to be associated with rift-related magmatism that represents the rifting of Rodinia (Lund et al., 2003; Balgord et al., 2013; Gaschnig et al., 2013; Keeley et al., 2013; Yonkee et al., 2014).

INITIAL ϵ_{Hf} FROM NEOPROTEROZOIC ORTHOGNEISS

We analyzed ten detrital grains with U-Pb ages 666–677 Ma from drill core at 238 m deep in U.S. Geological Survey (USGS) Drill Hole 142, in the lower Big Lost River drainage (Fig. 1; Table S4 [see footnote 4]; Mudge, 2016). Initial ϵ_{Hf} clusters near zero (Fig. 11), between 3.4 and –2.4. This intermediate value suggests that the Neoproterozoic granitoid plutons were partially melted from continental crust with a juvenile mantle component. This mixed origin is consistent with coeval rift-related volcanic rocks in the Pocatello Formation (Keeley et al., 2013).

DISCUSSION

Timing of Igneous Activity

Neoarchean

The felsic orthogneiss in the Pioneer Mountains was intruded in the Neoarchean. In all four samples, there is variable and at times significant radiogenic Pb loss, with the more concordant ages for two samples at ca. 2.66–2.67 Ga and the other two at ca. 2.60–2.61 Ga. The older $^{207}\text{Pb}/^{206}\text{Pb}$ age groupings are identical to intrusive ages from the Clearwater and Priest River complexes to the north as reported by Vervoort et al. (2015). The younger set of ages (2.60–2.61 Ga) from the Pioneer Mountains approach the ca. 2.57 Ga ages from xenoliths in Miocene volcanics from ~50 km to the southwest and ca. 2.50–2.60 Ga from Craters of the Moon National Monument to the south (Wolf et al., 2005). Furthermore, basement orthogneiss (Green Creek gneiss) from the Albion and Raft River Mountains immediately south of the Snake River Plain (Fig. 1) has yielded ages of ca. 2.57 Ga (Strickland et al., 2011).

Paleoproterozoic

Our new age of ca. 1.85 Ga for amphibolite in the middle paragneiss indicates that this unit, which was previously thought to have been deposited after ca. 1.45 Ga, locally contains metasedimentary rocks that are Paleoproterozoic or older. These ages also represent the southernmost exposures of rocks of this age that are prevalent to the north within both the Clearwater–Priest River block (Vervoort et al., 2015) and as inherited zircons within the Bitterroot lobe of the Idaho batholith (Gaschnig et al., 2013), as well as to the northeast along the Great Falls tectonic zone (e.g., Mueller et al., 2002, 2016; Vogl et al., 2004; Foster et al., 2006).

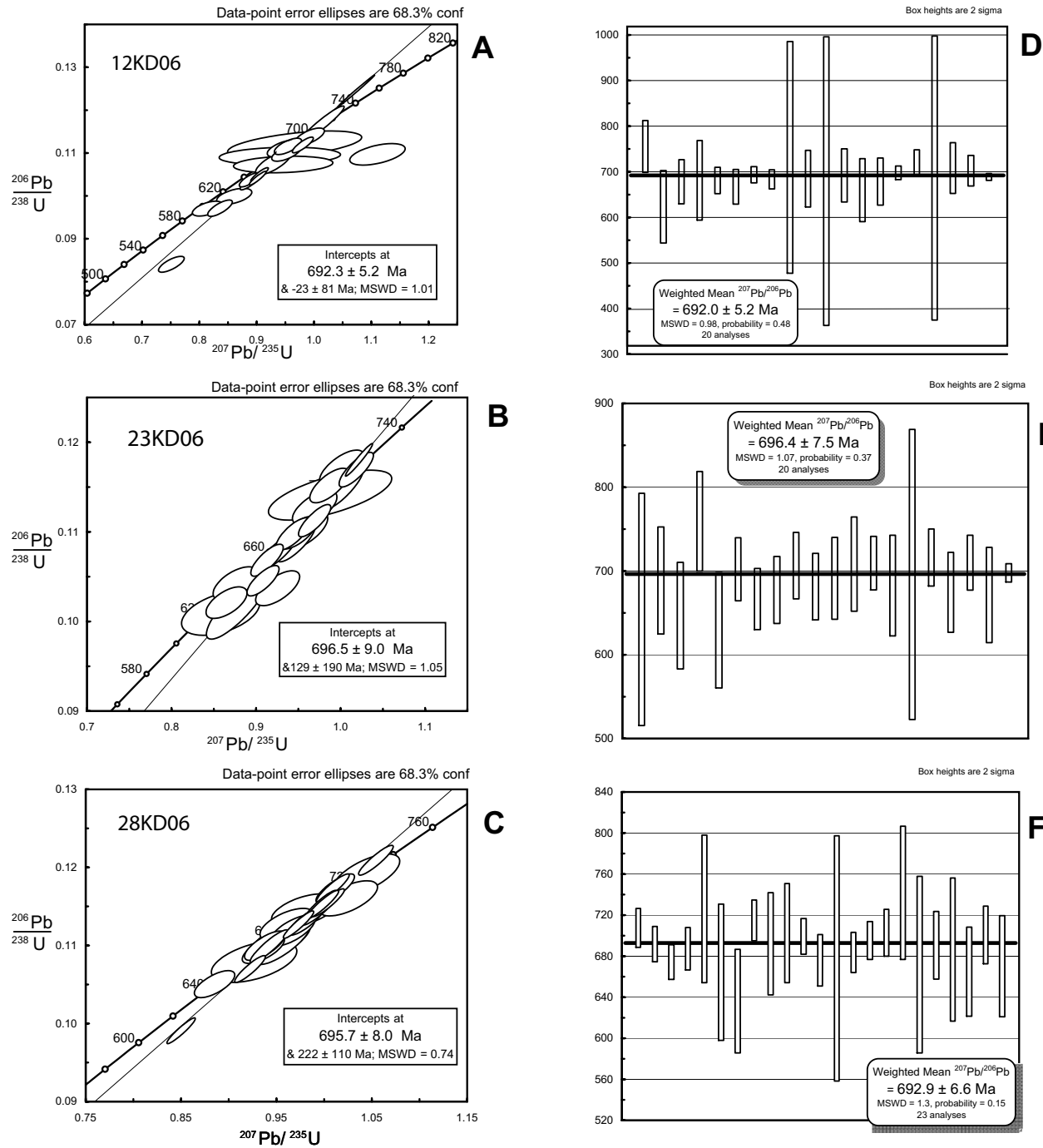


Figure 9. U-Pb zircon data from the upper orthogneiss (samples 12KD06, 23KD06, and 28KD06). (A) Sample 12KD06 concordia plot showing U-Pb analyses of dated zircon (Table S2L [see footnote 2]). Analyses plotted as 1 σ error ellipses. (B) Sample 23KD06, concordia plot showing U-Pb analyses of dated zircon (Table S2M [see footnote 2]). Analyses plotted as 1 σ error ellipses. (C) Sample 28KD06 concordia plot showing U-Pb analyses of dated zircon (Table S2N [see footnote 2]). Analyses plotted as 1 σ error ellipses. (D) Sample 12KD06 weighted average $^{207}\text{Pb}/^{206}\text{Pb}$ age. (E) Sample 23KD06 weighted average $^{207}\text{Pb}/^{206}\text{Pb}$ age. (F) Sample 28KD06 weighted average $^{207}\text{Pb}/^{206}\text{Pb}$ age. MSWD—mean square of weighted deviates; conf—confidence.

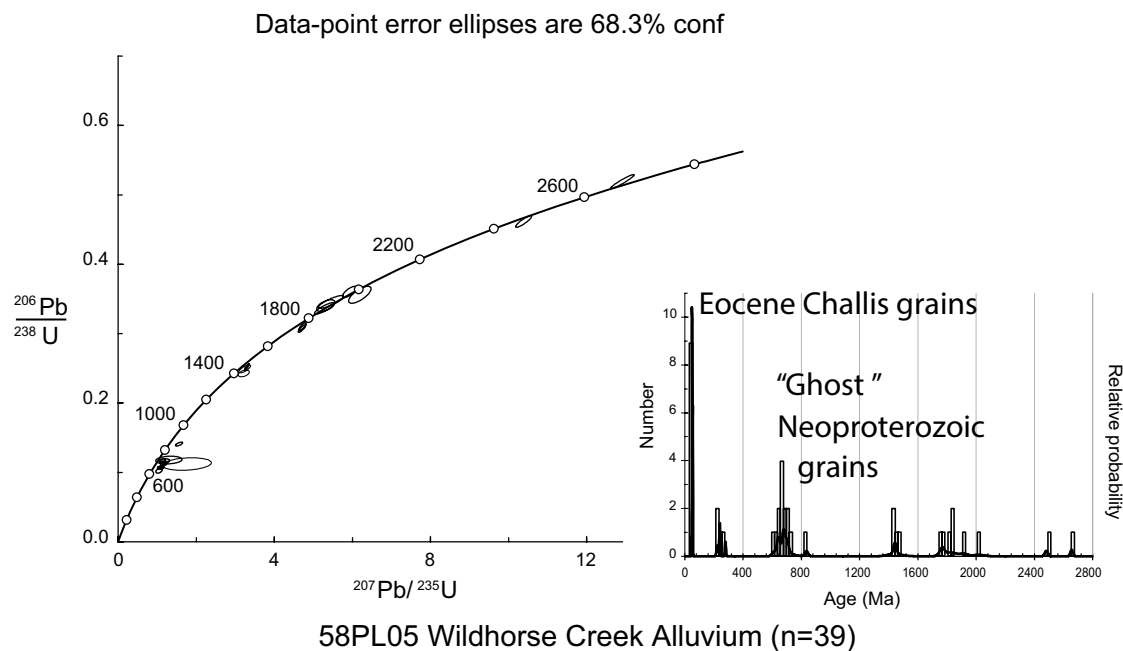


Figure 10. Detrital-zircon data (Wetherill concordia plot and probability density plot) from Holocene alluvium in Wildhorse Creek (sample 58PL05, Table S2A [see footnote 2]), n = 39. 25% of the grains are “ghosts,” ca. 700 Ma, an age not previously reported from the Pioneer Mountains. The two Archean ages are less discordant than grains in the source rock in the Wildhorse gneiss perhaps because discordant grains have lower likelihood of surviving stream transport; conf—confidence.

The association of ca. 1.85 Ga gneisses with 2.6–2.7 Ga gneisses appears to be common throughout limited exposures and xenoliths of the Medicine Hat block (Foster et al., 2006, 2012; Gifford et al., 2012; Vervoort et al., 2015) suggesting a relationship between the basement of the Grouse Creek and Medicine Hat blocks. Although we have only dated one sample of this age thus far, we note that there is less than 1000 m of pre-Mesoproterozoic structural section (Archean felsic orthogneiss and part of the middle paragneiss) exposed within the PMCC, providing a very limited view of the lowest basement.

Neoproterozoic

The 695 Ma orthogneiss is of the same age as Cryogenian volcanic rocks at Edwardsburg 170 km to the northwest (Lund et al., 2003, 2010). The ages also overlap with zircon populations in epiclastic volcanic sandstones of the Cryogenian Pocatello Formation south of the Snake River Plain (Keeley et al., 2013). Gaschnig et al. (2013) reported a significant component of inherited zircons with a peak age of ca. 670 Ma from the southern lobe of the Idaho Batholith. Yonkee et al. (2014) proposed that these magmatic rocks are related to rifting of Laurentia and the opening of the paleo-Pacific Ocean.

To the west in the Atlanta lobe of the Cretaceous Idaho batholith, Gaschnig et al. (2013) found a population of inherited zircons with an age peak of ca.

2.55 Ga, as well as a smaller population at ca. 671 Ma. They interpreted these inherited zircons as being derived from melting of an igneous protolith, rather than as detrital zircons from metasedimentary rocks. At House Mountain (Fig. 1), along the South Fork Boise River 100 km southwest of the PMCC, Cryogenian (725 Ma) orthogneiss intrudes Archean orthogneiss with an age of 2.55 Ga (Alexander et al., 2006; Alexander, 2007; Schmitz, 2011). This growing database of basement ages suggests that Neoproterozoic crust intruded by Neoproterozoic granitoids is present along a north-south distance of >500 km along the southwest edge of Laurentia (Fig. 1). The ages of these Neoproterozoic orthogneisses span a period of ~100 m.y.

Depositional History and Sediment Sources

Lower and Middle Paragneiss Units

The data from the lower paragneiss samples (Fig. 5) suggest deposition after ca. 2.5 Ga, and for sample 1AC09, the data suggest deposition after 1.7 Ga. Because of the differing detrital-zircon spectra, we suggest that several stratigraphic units are present. The age of ca. 1850 Ma from amphibolite within the middle paragneiss suggests that part of this package is Paleoproterozoic or older and must be more structurally complex than previously thought (Link et al., 2010).

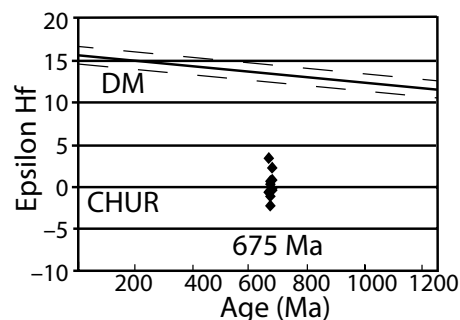


Figure 11. ϵ Hf plot for 675 Ma zircons in Big Lost River alluvium. These grains are interpreted to come from the Neoproterozoic orthogneiss in the Pioneer Mountains, and the Hf isotopic values thus reflect the evolved Precambrian crust from which these plutons were partially melted. CHUR—chondritic uniform reservoir; DM—depleted mantle.

We compared the detrital signatures of several of the PMCC units and Precambrian quartzites regionally (Fig. 12). Three samples of the lower paragneiss of the Wildhorse complex contain Archean detrital zircons with a range in ages from 2.5 to 3.3 Ga (two samples shown in Fig. 12E). This distribution does not resemble any part of the Lemhi Group or Belt Supergroup (Figs. 12A and 12B) but is similar to detrital-zircon patterns reported from the Cryogenian schist of the Upper Narrows (Fig. 12F) of the Raft River Range (Yonkee et al., 2014).

One sample of quartzite in the lower paragneiss (1AC09) contains a small population of concordant zircons with ages near 1710 Ma (see Table S2B [see footnote 2]). This age is similar to the largest age peak in the Lawson Creek, Swauger, and Apple Creek formations (Fig. 12A), the upper strata of the Lemhi subbasin of the Belt Supergroup.

Meta-Belt Supergroup

The middle and upper paragneiss units (Figs. 12C and 12D) contain detrital zircons as young as ca. 1400–1450 Ma indicating that the strata are Mesoproterozoic or Neoproterozoic in age; the upper paragneiss and at least part of the middle paragneiss are intruded by ca. 695 Ma orthogneiss, providing a minimum age of deposition in those units.

The 1800–1450 Ma detrital zircons in the middle and upper paragneiss units (Figs. 12C and 12D) span a similar age range to those in Lemhi Group and Belt Supergroup exposed to the north (Figs. 12A and 12B). We propose that these paragneiss units represent metamorphosed strata from the Lemhi subbasin of the Belt Supergroup and that the southern edge of the Belt basin extended at least as far south as the Pioneer Mountains. No evidence of Mesoproterozoic Belt Supergroup strata has been found south of the Pioneer Mountains, on the south side of the Snake River Plain.

Regional Basement Relations

Wildhorse complex orthogneiss has a similar 2.6 Ga Neoproterozoic age as granites of the Grouse Creek block. The northwestern Wyoming province has metasedimentary rocks older than 3 Ga (Foster et al., 2006). We do not find evidence in the Wildhorse gneiss for pre-2.6 Ga magmatic rocks and southwest structural trends predicted by Sims et al. (2004, 2005). These authors recognize northeast-striking aeromagnetic discontinuities in central Idaho that are interpreted to continue along strike into Archean terranes of southwest Montana. Extension of the Wyoming province southwestward would suggest that the Archean rocks under central Idaho should contain Mesoarchean amphibolite or granulite-grade metavolcanic and metasedimentary rocks. We have found no such ancient strata in the Pioneer Mountains.

Paleoproterozoic rocks are present in the Wildhorse gneiss. The age of ca. 1850 Ma from amphibolite within the middle paragneiss suggests that part of this package is Paleoproterozoic or older and more structurally complex than previously thought (Link et al., 2010). This age overlaps 2.45 and 1.8–1.9 Ga Paleoproterozoic (Farmington zone) metavolcanic rocks dated in the Tendoy Mountains, Montana (Fig. 1; Kellogg et al., 2003; Mueller et al., 2016) and the Coyote Creek quadrangle (Sherwin et al., 2016).

CONCLUSIONS

This paper establishes several geochronologic and tectonic geologic relations in the Pioneer Mountains.

- (1) We elucidate age relations between lithologic units in the Wildhorse complex. These include 2.6 Ga Neoproterozoic orthogneiss of the Grouse Creek block, 1.8 Ga Paleoproterozoic amphibolite, 1.45 Ga Mesoproterozoic paragneiss, and 695 Ma Neoproterozoic orthogneiss.
- (2) We clarify tectonic relationships between the Grouse Creek block and neighboring Archean Wyoming and Medicine Hat blocks and Paleoproterozoic Great Falls tectonic zone. The Pioneer Mountains represent a northern extension of the Grouse Creek block north of the Snake River Plain against the southern margin of the Great Falls tectonic zone on the north and the Farmington zone on the east.
- (3) We identify Mesoproterozoic depositional ages and provenance similarities that support a southward extension of the Mesoproterozoic Belt Basin to the Pioneer Mountains.
- (4) We identify zircon-rich Neoproterozoic intrusive rocks (metamorphosed to orthogneiss) in the Wildhorse complex. These rocks likely record rifting along the western margin of Laurentia and are the source for 710–650 Ma detrital-zircon populations from the Lost River drainage.
- (5) Initial ϵ Hf values from 675 Ma detrital zircons of the lower Big Lost River reflect a mixture between older continental material and more juvenile mantle-derived magma as the source for the Neoproterozoic orthogneiss. Thus if there was an Archean Grouse Creek block component, there was also a juvenile mantle component.

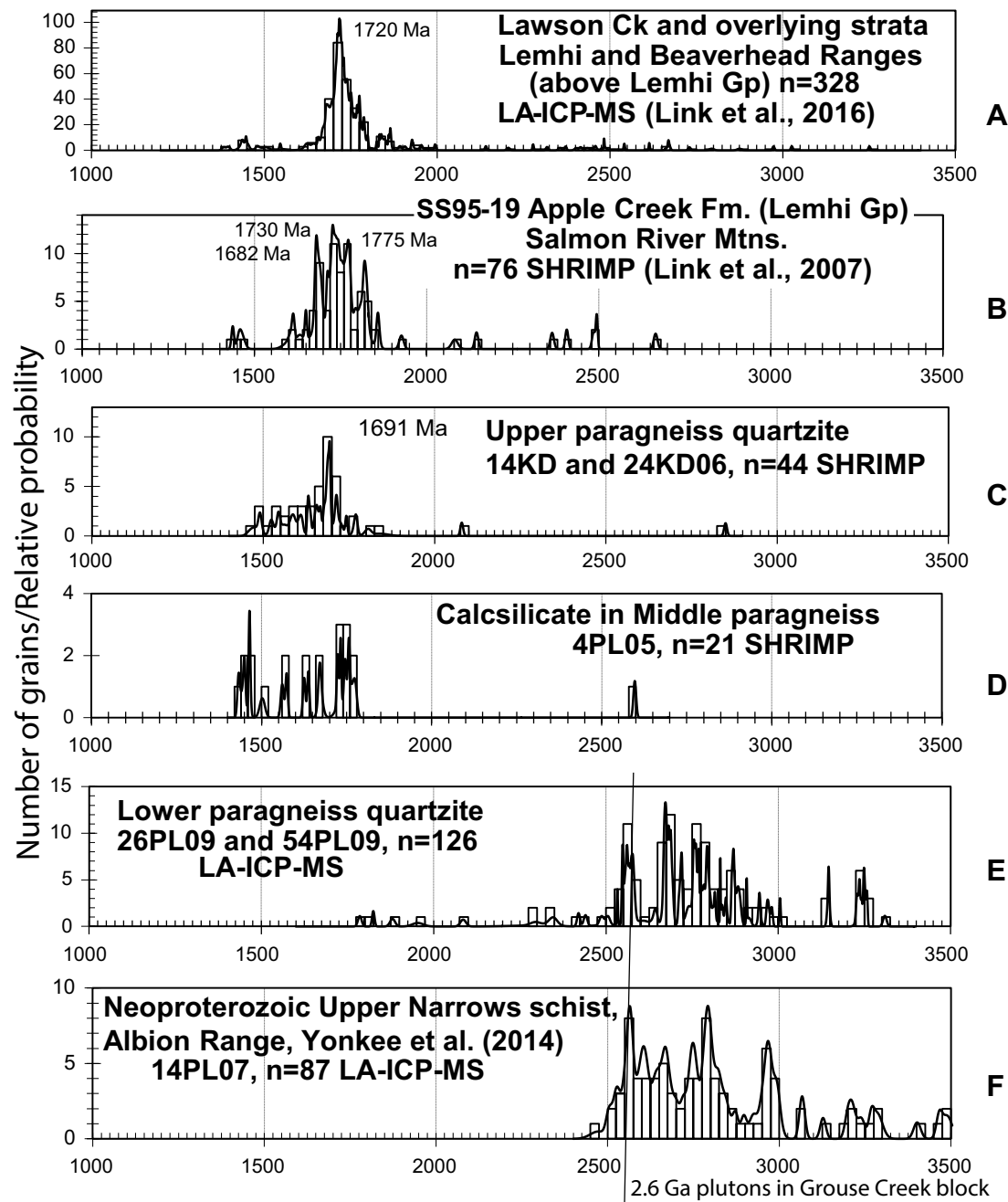


Figure 12. Probability density plots of selected metasediments from the Pioneer Mountains, the Belt Supergroup and one sample from the Albion Range, Idaho. (A) Lawson Creek and overlying strata, Lemhi and Beaverhead Ranges (Link et al., 2016). (B) Apple Creek Formation, Blackbird district, Salmon River Mountains (sample SS95-19), Link et al. (2007). (C) Upper paragneiss quartzite (samples 14KD and 24KD06); (D) middle paragneiss calc-silicate (sample 4PL05). (E) Lower paragneiss quartzite (samples 26PL09 and 54PL09). (F) Neoproterozoic Upper Narrows schist, Raft River Range (Yonkee et al., 2014; sample 14PL07).

ACKNOWLEDGMENTS

Art Snoke has been a role model and friend for 40 years. This research was supported by National Science Foundation grants EAR 05-10980 and 08-38425 and U.S. Geological Survey grant G14AC00136. Logistical support was provided by the Idaho State University Geology field camp at Lost River Field Station. Diana Boyack provided invaluable help with illustrations. Reviews by Paul Mueller, Joshua Schwartz, and two anonymous reviewers were extremely helpful.

REFERENCES CITED

- Alcock, J., and Muller, P., 2012, A Paleoproterozoic sedimentary basin within the Wyoming craton exposed in the Ruby Range, SW Montana: Identified by field relations and geochronology: *Northwest Geology*, v. 41, p. 47–62.
- Alcock, J., Muller, P.D., and Jercinovic, M.J., 2013, Monazite ages and pressure-temperature-time paths from anatectites in the southern Ruby Range, Montana, USA: Evidence for delamination, ultramafic magmatism, and rapid uplift at ca. 1780 Ma: *Canadian Journal of Earth Sciences*, v. 50, no. 11, p. 1069–1084, doi:10.1139/cjes-2013-0035.
- Alexander, J.T., 2007, Geochronology of the House Mountain Gneiss complex in the Atlanta Lobe of the Idaho Batholith [M.S. thesis]: Boise, Idaho, Boise State University, 95 p.
- Alexander, J.T., Schmitz, M.D., and Northrup, C.J., 2006, Preliminary U/Pb zircon data from the House Mountain metamorphic complex in the Atlanta lobe of the Idaho batholith: *Geological Society of America, Abstracts with Programs*, v. 38, no. 7, p. 483.
- Bahlburg, H., Vervoort, J.D., DuFrane, S.A., Carlotto, V., Reimann, C., and Cárdenas, J., 2011, The U-Pb and Hf isotope evidence of detrital zircons of the Ordovician Ollantaytambo Formation, southern Peru, and the Ordovician provenance and paleogeography of southern Peru and northern Bolivia: *Journal of South American Earth Sciences*, v. 32, p. 196–209, doi:10.1016/j.jsames.2011.07.002.
- Balgord, E.A., Yonkee, W.A., Link, P.K., and Fanning, C.M., 2013, Stratigraphic, geochronologic, and geochemical record of the Cryogenian Perry Canyon Formation, northern Utah: Implications for Rodinian rifting and snowball Earth glaciation: *Geological Society of America Bulletin*, v. 125, no 9/10, p. 1423–1467; doi:10.1130/B30860.1.
- Beranek, L.P., Link, P.K., and Fanning, C.M., 2016, Detrital zircon record of mid-Paleozoic convergent margin activity in the northern U.S. Rocky Mountains: Implications for the Antler orogeny and early evolution of the North American Cordillera: *Lithosphere*, v. 8, no. 5, doi: 10.1130/L557.1.
- Burmester, R.F., Lonn, J.D., Lewis, R.S., and McFadden, M.D., 2016, Stratigraphy of the Lemhi subbasin of the Belt Supergroup, in MacLean, J.S., and Sears, J.W., eds., *Belt Basin: Window to Mesoproterozoic Earth: Geological Society of America Special Paper 522*, p. 121–137, doi:10.1130/2016.2522(05).
- Cameron, A., 2010, Geochronology of the lower Wildhorse Gneiss complex, Pioneer Mountains, Custer County, Idaho [B.S. thesis]: Pocatello, Idaho State University, 43 p.
- Cecil, M.R., Gehrels, G.E., Ducea, M.N., and Patchett, P.J., 2011, U-Pb-Hf characterization of the central Coast Mountains batholith: Implications for petrogenesis and crustal architecture: *Lithosphere*, v. 3, p. 247–260, doi:10.1130/L134.1.
- Dover, J.H., 1969, Bedrock geology of the Pioneer Mountains, Blaine and Custer Counties, central Idaho: Idaho Bureau of Mines and Geology Pamphlet 142, 66 p.
- Dover, J.H., 1981, Geology of the Boulder-Pioneer wilderness study area, Chapter A, in Simons, F.S., Dover, J.H., Mabey, D.R., Tucek, E.T., and Ridenour, J., eds., *Mineral Resources of the Boulder-Pioneer Study Area, Blaine and Custer Counties, Idaho: U.S. Geological Survey Bulletin 1497*, p. 15–75.
- Dover, J.H., 1983, Geologic map and sections of the central Pioneer Mountains, Blaine and Custer Counties, central Idaho: U.S. Geological Survey Miscellaneous Investigations Series Map I-1319, 1:48,000, 2 sheets.
- Durk, K., 2007, Geochronology of part of the Wildhorse Gneiss complex, Pioneer Mountains, Custer County Idaho [senior thesis]: Pocatello, Idaho State University, 38 p.
- Egger, A.E., Dumitru, T.A., Miller, E.L., Savage, C.F.I., and Wooden, J.L., 2003, Timing and nature of Tertiary plutonism and extension in the Grouse Creek Mountains, Utah: *International Geology Review*, v. 45, no. 6, p. 497–532, doi:10.2747/0020-6814.45.6.497.
- Foster, D.A., and Fanning, C.M., 1997, Geochronology of the northern Idaho Batholith and the Bitterroot metamorphic core complex; magmatism preceding and contemporaneous with extension: *Geological Society of America Bulletin*, v. 109, no. 4, p. 379–394, doi:10.1130/0016-7606(1997)109<0379:GOTNIB>2.3.CO;2.
- Foster, D.A., Mueller, P.A., Mogk, D.W., Wooden, J.L., and Vogl, J.J., 2006, Proterozoic evolution of the western margin of the Wyoming craton: Implications for the tectonic and magmatic evolution of the northern Rocky Mountains: *Canadian Journal of Earth Sciences*, v. 43, p. 1601–1619, doi:10.1139/e06-052.
- Foster, D.A., Mueller, P.A., Heatherington, A., Gifford, J.N., and Kalakay, T.J., 2012, Lu-Hf systematics of magmatic zircons reveal a Proterozoic crustal boundary under the Cretaceous Pioneer batholith, Montana: *Lithos*, v. 142–143, p. 216–225, doi:10.1016/j.lithos.2012.03.005.
- Gaschnig, R.M., Vervoort, J.D., Lewis, R.S., and Tikoff, B., 2013, Probing for Proterozoic and Archean crust in the northern U.S. Cordillera with inherited zircon from the Idaho batholith: *Geological Society of America Bulletin*, v. 125, no. 1/2, p. 73–88, doi:10.1130/B30583.1.
- Gehrels, G., and Pecha, M., 2014, Detrital zircon U-Pb geochronology and Hf isotope geochemistry of Paleozoic and Triassic passive margin strata of western North America: *Geosphere*, v. 10, no. 1, p. 49–65, doi:10.1130/GES00889.1.
- Gifford, J.N., Mueller, P.A., Foster, D.A., and Mogk, D.W., 2012, At the cratonic crossroads: A geochronologic and geochemical perspective of the Little Rocky Mountains, Montana: San Francisco, California, American Geophysical Union Fall Meeting, Abstract 1481382.
- Gifford, J.N., Mueller, P.A., Foster, D.A., and Mogk, D.W., 2014, Precambrian crustal evolution in the Great Falls tectonic zone: Insights from xenoliths from the Montana Alkali Province: *The Journal of Geology*, v. 122, p. 531–548, doi:10.1086/677262.
- Goodge, J.W., and Vervoort, J.D., 2006, Origin of Mesoproterozoic A-type granites in Laurentia; Hf isotope evidence: *Earth and Planetary Science Letters*, v. 243, p. 711–731, doi:10.1016/j.epsl.2006.01.040.
- Harrison, J.E., Griggs, A.B., and Wells, J.D., 1974, Tectonic features of the Precambrian Belt basin and their influence on post-Belt structures: U.S. Geological Survey Professional Paper 719, 24 p.
- Hodges, M.K.V., Link, P.K., and Fanning, C.M., 2009, Drainage disruption by basaltic lava fields along the Snake River Plain hotspot track: Detrital zircon evidence from drill core constrains the course of the Pliocene Big Lost River: *Journal of Volcanology and Geothermal Research*, v. 188, p. 237–249, doi:10.1016/j.jvolgeores.2009.08.019.
- Keeley, J.A., Link, P.K., Fanning, C.M., and Schmitz, M.D., 2013, Pre- to synglacial rift-related volcanism in the Neoproterozoic (Cryogenian) Pocatello Formation, SE Idaho: New SHRIMP and CA-ID-TIMS constraints: *Lithosphere*, v. 5, no. 1, p. 128–150, doi:10.1130/L226.1.
- Kellogg, K.S., Snee, L.W., and Unruh, D.M., 2003, The Mesoproterozoic Beaverhead impact structure and its tectonic setting, Montana-Idaho: $^{40}\text{Ar}/^{39}\text{Ar}$ and U-Pb isotopic constraints: *The Journal of Geology*, v. 111, p. 639–652, doi:10.1086/378339.
- Kinny, P.D., and Maas, R., 2003, Lu-Hf and Sm-Nd isotope systems in zircon: Reviews in Mineralogy and Geochemistry, v. 53, p. 327–341, doi:10.2113/0530327.
- Leeman, W.P., Menzies, M.A., Matty, D.J., and Embree, G.F., 1985, Strontium, neodymium, and lead isotope compositions of deep crustal xenoliths from the Snake River Plain: Evidence for Archean basement: *Earth and Planetary Science Letters*, v. 75, p. 354–368, doi:10.1016/0012-821X(85)90179-7.
- Link, P.K., Mahoney, J.B., Batatian, L.D., Bruner, D.J., and Williams, F., 1995, Stratigraphic setting of sediment-hosted mineral deposits in the eastern part of the Hailey 1° × 2° quadrangle, and part of the southern part of the Challis 1° × 2° quadrangle, south-central Idaho: U.S. Geological Survey Bulletin 2064-C, p. C1–C33.
- Link, P.K., Warren, I., Preacher, J.M., and Skipp, B., 1996, Stratigraphic analysis and interpretation of the Copper Basin Group, McGowan Creek Formation and White Knob Limestone, south-central Idaho, in Longman, M.W., and Sonnenfeld, M.D., eds., *Paleozoic Systems of the Rocky Mountain Region: Rocky Mountain Section, SEPM (Society for Sedimentary Geology)*, p. 117–144.
- Link, P.K., Fanning, C.M., and Beranek, L.P., 2005, Reliability and longitudinal change of detrital-zircon age spectra in the Snake River system, Idaho and Wyoming: An example of reproducing the bumpy barcode: *Sedimentary Geology*, v. 182, p. 101–142, doi:10.1016/j.sedgeo.2005.07.012.
- Link, P.K., Fanning, C.M., Lund, K.I., and Aleinikoff, J.N., 2007, Detrital-zircon populations and provenance of Mesoproterozoic strata of east-central Idaho, U.S.A.: Correlation with the Belt Supergroup of southwest Montana, in Link, P.K., and Lewis, R.S., eds., *Proterozoic Geology of Western North America and Siberia: SEPM (Society for Sedimentary Geology) Special Publication*, v. 86, p. 101–128, doi:10.2110/pec.07.86.0101.
- Link, P.K., Cameron, A., and Autenrieth-Durk, K., 2010, Tectonostratigraphy of the Wildhorse gneiss complex, Pioneer Mountains: Neoproterozoic orthogneiss and overlying Mesoproterozoic Lemhi Group overlie Albion Range Proterozoic quartzite: *Geological Society of America, Abstracts with Programs*, v. 42, no. 5, p. 415.
- Link, P.K., Mahon, R.C., Beranek, L.P., Campbell-Stone, E.A., and Lynds, R., 2014, Detrital zircon provenance of Pennsylvanian to Permian sandstones from the Wyoming craton and Wood River Basin, Idaho, U.S.A.: *Rocky Mountain Geology*, v. 49, no. 2, p. 115–136, doi:10.2113/rgsrocky.49.2.115.

- Link, P.K., Stewart, E.D., and Steel, T.S., Sherwin, J.-A., Hess, L.T., and McDonald, C., 2016, Detrital zircons in the Mesoproterozoic upper Belt Supergroup in the Pioneer, Beaverhead and Lemhi Ranges, MT and ID, *in* Maclean, J.S., and Sears, J.W., eds., *Belt Basin: Window to Mesoproterozoic Earth: Geological Society of America Special Paper 522*, p. 163–183, doi:10.1130/2016.2522(03).
- Ludwig, K.R., 2000, SQUID 1.00, A User's Manual: Berkeley, California, Berkeley Geochronology Center Special Publication no. 2.
- Ludwig, K.R., 2003, Isoplot/Ex 3.00: A geochronological toolkit for Microsoft Excel: Berkeley, Berkeley Geochronology Center Special Publication no. 4, 70 p.
- Lund, K., Aleinikoff, J.N., Evans, K.V., and Fanning, C.M., 2003, SHRIMP U-Pb geochronology of Neoproterozoic Windermere Supergroup, central Idaho: Implications for rifting of western Laurentia and synchronicity of Sturtian glacial deposits: *Geological Society of America Bulletin*, v. 115, no. 3, p. 349–372, doi:10.1130/0016-7606(2003)115<0349:SUPGON>2.0.CO;2.
- Lund, K., Aleinikoff, J.N., Evans, K.V., duBray, E.A., Dewitt, E.H., and Unruh, D.M., 2010, SHRIMP U-Pb dating of recurrent Cryogenian and Late Cambrian–Early Ordovician alkalic magmatism in central Idaho: Implications for Rodinian rift tectonics: *Geological Society of America Bulletin*, v. 122, no. 3/4, p. 430–453, doi:10.1130/B26565.1.
- Ma, Chong, Bergeron, P., Foster, D.A., Dutrow, B.L., Mueller, P.A., and Allen, C., 2016, Detrital-zircon geochronology of the Sawtooth metamorphic complex, Idaho: Evidence for metamorphosed lower Paleozoic shelf strata within the Idaho batholith: *Geosphere*, v. 12, no. 4, p. 1136–1153, doi:10.1130/GES01201.1.
- Mahoney, J.B., Link, P.K., Burton, B.R., Geslin, J.K., and O'Brien, J.P., 1991, Pennsylvanian and Permian Sun Valley Group: Wood River basin, south-central Idaho, *in* Cooper, J.D., and Stevens, C.H., eds., *Paleozoic Paleogeography of the Western United States—II: Pacific Section, SEPM (Society for Sedimentary Geology)*, v. 67, p. 551–580.
- McFadden, R.R., Mulch, A., Teysseier, C., and Heizler, M., 2015, Eocene extension and meteoric fluid flow in the Wildhorse detachment, Pioneer metamorphic core complex, Idaho: *Lithosphere*, v. 7, no. 4, p. 355–366, doi:10.1130/L429.1.
- Mudge, C.M., 2016, Properties of Pleistocene sediment in two wells in the west-central portion of the Big Lost Trough, Eastern Snake River Plain, Idaho National Laboratory Idaho [M.S. thesis]: Pocatello, Idaho State University, 121 p.
- Mueller, P.A., Heatherington, A.L., D'Arcy, K.A., Wooden, J.L., and Nutman, A.P., 1996, Contrasts between Sm-Nd whole-rock and U-Pb zircon systematics in the Tobacco Root batholith, Montana: Implications for the determination of crustal age provinces: *Tectonophysics*, v. 265, p. 169–179, doi:10.1016/S0040-1951(96)00151-5.
- Mueller, P.A., Heatherington, A.L., Kelly, D.M., Wooden, J.L., and Mogk, D.W., 2002, Paleoproterozoic crust within the Great Falls tectonic zone: Implications for the assembly of southern Laurentia: *Geology*, v. 30, no. 2, p. 127–130, doi:10.1130/0091-7613(2002)030<0127:PCWTGF>2.0.CO;2.
- Mueller, P.A., Wooden, J.L., Mogk, D.W., and Foster, D.A., 2011, Paleozoic evolution of the Farmington zone: Implications for terrane accretion in southwestern Laurentia: *Lithosphere*, v. 3, p. 401–408, doi:10.1130/L161.1.
- Mueller, P., Mogk, D., Wooden, J., and Spake, D., 2016, U-Pb ages of zircons from the Lower Belt Supergroup and proximal crystalline basement: Implications for the early evolution of the Belt Basin, *in* MacLean, J.S., and Sears, J.W., eds., *Belt Basin: Window to Mesoproterozoic Earth: Geological Society of America Special Paper 522*, p. 283–303, doi:10.1130/2016.2522(11).
- O'Neill, J.M., and Lopez, D.A., 1985, Character and regional significance of Great Falls tectonic zone, east-central Idaho and west-central Montana: *American Association of Petroleum Geologists Bulletin*, v. 69, no. 3, p. 437–447.
- O'Neill, R.L., and Pavlis, T.L., 1988, Superposition of Cenozoic extension on Mesozoic compressional structures in the Pioneer Mountains metamorphic core complex, central Idaho: *Geological Society of America Bulletin*, v. 100, p. 1833–1845, doi:10.1130/0016-7606(1988)100<1833:SOCEOM>2.3.CO;2.
- Ruppel, R.T., 1975, Precambrian Y sedimentary rocks in east-central Idaho: U.S. Geological Survey Professional Paper 889-A, 23 p.
- Schmitz, M.D., 2011, A window into the middle crust of the northern U.S. Cordillera at House Mountain, southern Idaho batholith: *Geological Society of America Abstracts with Programs*, v. 43, no. 4, p. 76.
- Shervais, J.W., 2006, The significance of subduction-related accretionary complexes in early Earth processes, *in* Reimold, W.U., and Gibson, R.L., eds., *Processes on the Early Earth: Geological Society of America Special Paper 405*, p. 173–192, doi:10.1130/2006.2405(10).
- Sherwin, J., Younggren, E.B., Link, P.K., and Gaschnig, R.M., 2016, Geologic map of the Coyote Creek 7.5' quadrangle, southwest Montana: Montana Bureau of Mines and Geology Map 67, scale 1:24,000.
- Silverberg, D.S., 1990, The tectonic evolution of the Pioneer metamorphic core complex south-central, Idaho [Ph.D. thesis]: Cambridge, Massachusetts, Massachusetts Institute of Technology, 280 p.
- Sims, P.K., O'Neill, J.M., Bankey, V., and Anderson, E., 2004, Precambrian basement geologic map of Montana—An interpretation of aeromagnetic anomalies: U.S. Geological Survey Scientific Investigations Map 2829, scale 1,000,000.
- Sims, P.K., Lund, K., and Anderson, E., 2005, Precambrian crystalline basement map of Idaho—An interpretation of aeromagnetic anomalies: U.S. Geological Survey Scientific Investigations Map 2884, scale 1:1,000,000.
- Stewart, E.D., Link, P.K., Fanning, C.M., Frost, C.D., and McCurry, M., 2010, Paleogeographic implications of non-North American sediment in the Mesoproterozoic upper Belt Supergroup and Lemhi Group, Idaho and Montana, USA: *Geology*, v. 38, no. 10, p. 927–930, doi:10.1130/G31194.1.
- Strickland, A., Miller, E.L., and Wooden, J.L., 2011, The timing of Tertiary metamorphism and deformation in the Albion–Raft River–Grouse Creek metamorphic core complex, Utah and Idaho: *The Journal of Geology*, v. 119, no. 2, p. 185–206, doi:10.1086/658294.
- Toth, M.I., and Stacey, J.S., 1992, Constraints on the formation of the Bitterroot lobe of the Idaho batholith, Idaho and Montana, from U-Pb zircon geochronology and feldspar Pb isotopic data: U.S. Geological Survey Bulletin 2008, 14 p.
- Umpleby, J.B., Westgate, L.G., Ross, C.P., and Hewett, D.F., 1930, Geology and ore deposits of the Wood river region, Idaho, with a description of the Minnie Moore and nearby mines: U.S. Geological Survey Bulletin 814, 250 p.
- Vervoort, J.D., Lewis, R.S., Fisher, R.C., Gaschnig, R.M., Jansen, A.C., and Brewer, R., 2015, Neoproterozoic and Paleoproterozoic crystalline basement rocks of north-central Idaho: Constraints on the formation of western Laurentia: *Geological Society of America Bulletin*, v. 128, no. 1–2, p. 94–109, doi:10.1130/B31150.1.
- Vogl, J.J., Foster, D.A., Mueller, P.A., Wooden, J.L., and Mogk, D.W., 2004, Lithology and age of pre-Belt Precambrian basement in the Little Belt Mountains, Montana: Implications for the role of the Great Falls tectonic zone in the Paleoproterozoic assembly of North America: *Northwest Geology*, v. 33, p. 15–34.
- Vogl, J.J., Foster, D.A., Fanning, M.A., Kent, K.A., Rodgers, D.W., and Diedesch, T., 2012, Timing of extension in the Pioneer metamorphic core complex with implications for the spatial-temporal pattern of Cenozoic extension and exhumation in the northern U.S. Cordillera: *Tectonics*, v. 31, TC1008, doi:10.1029/2011TC002981.
- Vogl, J.J., Min, K., Carmenate, A., Foster, D.A., and Marsellos, A., 2014, Miocene regional hotspot-related uplift, exhumation, and extension north of the Snake River Plain: Evidence from apatite (U-Th)/He thermochronology: *Lithosphere*, v. 6, p. 108–123, doi:10.1130/L308.1.
- Williams, I.S., 1998, U-Th-Pb Geochronology by Ion Microprobe, *in* McKibben, M.A., Shanks, W.C., III, and Ridley, W.I., eds., *Applications of Microanalytical Techniques to Understanding Mineralizing Processes: Reviews in Economic Geology*, v. 7, p. 1–35.
- Winston, D., and Link, P.K., 1993, Middle Proterozoic rocks of Montana, Idaho, and Washington: The Belt Supergroup, *in* Reed, J., Sims, P., Houston, R., Rankin, D., Link, P., Van Schmus, R., and Bickford, P., eds., *Precambrian of the Conterminous United States: Boulder, Colorado, Geological Society of America, The Geology of North America*, v. C-3, p. 487–521.
- Winston, D., Link, P.K., and Hathaway, N., 1999, The Yellowjacket is not the Prichard and other heresies: Belt Supergroup correlations, structure and paleogeography, east-central Idaho, *in* Hughes, S.S., and Thackray, G.D., eds., *Guidebook to the Geology of Eastern Idaho: Pocatello, Idaho Museum of Natural History*, p. 3–20.
- Wolf, D.E., Leeman, W.P., and Vervoort, J.D., 2005, U-Pb zircon geochronology of crustal xenoliths confirms presence of Archean basement beneath the central and eastern Snake River Plain: *Geological Society of America Abstracts with Programs*, v. 37, no. 7, p. 60.
- Worl, R.G., Link, P.K., Winkler, G.R., and Johnson, K.M., eds., 1995, *Geology and Mineral Resources of the Hailey 1° x 2° Quadrangle and the Western Part of the Idaho Falls 1° x 2° Quadrangle, Idaho: U.S. Geological Survey Bulletin 2064*, v.1, chap. A–R.
- Wust, S.L., 1986, Extensional deformation with northwest vergence, Pioneer core complex, central, Idaho: *Geology*, v. 14, p. 712–714, doi:10.1130/0091-7613(1986)14<712:EDWNVF>2.0.CO;2.
- Yonkee, W.A., Dehler, C.D., Link, P.K., Balgord, E.A., Keeley, J.A., Hayes, D.S., Wells, M.L., Fanning, C.M., and Johnson, S.M., 2014, Tectono-stratigraphic framework of Neoproterozoic to Cambrian strata, west-central U.S.: Protracted rifting, glaciation, and evolution of the North American Cordilleran margin: *Earth-Science Reviews*, v. 136, p. 59–95, doi:10.1016/j.earscirev.2014.05.004.